SPACE SHUTTLE MAIN ENGINE HIGH PRESSURE
FUEL TURBOPUMP TURBINE BLADE CRACKING

By Henry Lee

Structures and Dynamics Laboratory
Science and Engineering Directorate

May 1988

1. REPORT NO. NASA TM-100327	2. GOVERNMENT ACCESSION NO.	3. RECIPIENT'S CATALOG NO.
4. TITLE AND SUBTITLE Space Shuttle Main Engine High Pressure Fuel Turbopump Turbine Blade Cracking		5. REPORT DATE May 1988
		6. PERFORMING ORGANIZATION CODE
7. AUTHOR(S) Henry Lee		8. PERFORMING ORGANIZATION REPORT #
9. PERFORMING ORGANIZATION NAME AND ADDRESS George C. Marshall Space Flight Center Marshall Space Flight Center, Alabama 35812		10. WORK UNIT NO.
		11. CONTRACT OR GRANT NO.
12. SPONSORING AGENCY NAME AND ADDRESS National Aeronautics and Space Administration Washington, D.C. 20546		13. TYPE OF REPORT & PERIOD COVERED Technical Memorandum
		14. SPONSORING AGENCY CODE

15. SUPPLEMENTARY NOTES

Prepared by Structures and Dynamics Laboratory, Science and Engineering Directorate.

16. ABSTRACT

This report presents the analytical results from two-dimensional (2D) and three-dimensional (3D) finite element model investigations into the cracking of Space Shuttle Main Engine (SSME) High Pressure Fuel Turbopump (HPFTP) first- and second-stage turbine blades. Specifically, the initiation causes for transverse cracks on the pressure side of the first-stage blade fir tree lobes and face/corner cracks on the downstream fir tree face of the second-stage blade are evaluated.

Because the blade material, MAR-M-246 Hf (DS), is highly susceptible to hydrogen embrittlement in the -100°F to 400°F thermal environment, a steady-state condition (Full power level - 109%) rather than a start-up or shut-down transient was considered to be the most likely candidate for generating a high-strain state in the fir tree areas.

Results of the analyses yielded strain levels on both first- and second-stage blade fir tree regions that are of a magnitude to cause hydrogen assisted low cycle fatigue cracking. Also evident from the analysis is that a positive margin against fir tree cracking exists for the planned design modifications, which include shot peening for both first- and second-stage blade fir tree areas.

17. KEY WORDS Turbine blade Hydrogen embrittlement	18. DISTRIBUTION STATEMENT Unclassified — Unlimited

19. SECURITY CLASSIF. (of this report) Unclassified	20. SECURITY CLASSIF. (of this page) Unclassified	21. NO. OF PAGES 57	22. PRICE NTIS

MSFC - Form 3292 (May 1969)

TABLE OF CONTENTS

PAGE _II_ INTENTIONALLY BLANK

LIST OF ILLUSTRATIONS

LIST OF ILLUSTRATIONS (Concluded)

LIST OF TABLES

TECHNICAL MEMORANDUM

SPACE SHUTTLE MAIN ENGINE HIGH PRESSURE FUEL
TURBOPUMP TURBINE BLADE CRACKING

SUMMARY

To determine the state of strain that exists in the fir tree area of both the first- and second-stage turbine blades in the Space Shuttle Main Engine (SSME) High Pressure Fuel Turbopump Turbine (HPFTP), large two-dimensional (2D) and three-dimensional (3D) finite element models of the blades and disks were developed on the Marshall Space Flight Center (MSFC) Intergraph Interactive Graphics Design System (IGDS) and translated into the ANSYS structural analysis computer program. The program was then executed on the MSFC Cray X-MP/44 system. Because the cracking was thought to be hydrogen assisted low-cycle fatigue of the MAR-M-246(Hf) DS blade material, a steady-state condition known as full power level (FPL-109%) rather than a start-up or shut-down transient was utilized as the baseline environment.

The foundational aerodynamic analyses were accomplished by the MSFC Computational Fluid Dynamics Branch (ED32). This critical phase supplied the airfoil pressure distributions, heat transfer coefficients, hot gas temperatures, and other pertinent boundary data essential for 3D thermo-structural analyses. The airfoil pressures were computationally generated for every structural model node point so that complex interpolation was not necessary. Since the blade temperature profile plays such a significant role in the determination of strain levels, the MSFC Thermal Systems Branch (EL56) utilized these data along with the aforementioned ANSYS 3D structural model in developing nodal temperatures. This huge analysis task allowed these generated temperatures to be directly applied to the structural model without any interpolation or extrapolation of data. The entire FPL (109%) steady-state environment was then applied to the model as (1) airfoil pressure (generating 128,000 in.-lb torque), (2) blade temperature, (3) speed (36,595 rpm), and (4) substructured disk boundary interface.

Although there have been numerous types of cracks develop on both stages of the HPFTP, this study dealt specifically with transverse cracks on the pressure side of the first-stage blade fir tree lobe, and face/corner cracks on the downstream fir tree face of the second-stage blade. Analytically predicted strain values for both first- and second-stage blade fir tree areas were of a magnitude that would implicate hydrogen embrittlement as the crack initiator. Recent material tests have indicated that the blade parent material can crack in the presence of 5000 psi hydrogen with zero plastic strain (yield strain is near 0.57 percent) in the temperature range from -100°F to 400°F. This same testing also revealed that shot peening increases the strain range to 1.37 percent for the blade surface. Since some crack initiations are at carbides and pores on the surface, the acceptable microporosity size was reduced from 0.015 to 0.005 in. Other modifications include stress relieving the blades prior to shot peening, providing more generous radii on fir tree corners, and some fit-up changes to improve the load sharing between lobes. This latter change was analytically studied using 2D models, and revealed increases in strain of 10 to 35 percent in the fir tree neck regions with a geometric lobe tolerance of 0.00025 in. The design modifications discussed above analytically provide a factor of safety of 2.09 for the first-stage necks and a factor of safety of 1.69 for the second-stage

face/corner against hydrogen assisted crack initiations. In addition, the low cycle fatigue (LCF) life of the first stage was conservatively found to be 700 cycles. For the second stage, the LCF life was 175 cycles.

INTRODUCTION

The SSME HPFTP turbine is a two stage reaction turbine with curvic coupled rotors powered with 5500 psi hydrogen-rich steam generated by a fuel preburner producing hot gas temperatures near 2000°R (1540°F). Gaseous hydrogen flows as coolant beneath the platform, passing between the blades and disk in the fir tree area at 140°R (-320°F) on the first stage and 1400°R (940°F) on the second stage. Figure 1 shows a cross-section of this turbine. At full power level (FPL-109% of rated power level), the machine produces some 74,000 horsepower (HP) while rotating at 36,595 rpm. With 63 blades on the first-stage rotor and 59 blades on the second-stage rotor, this translates to over 600 HP per blade [1].

The SSME HPFTP first- and second-stage blades (Fig. 2) have historically experienced a large variation in types and location of cracks. An example of some of the cracks presently being tracked and requiring continual surveillance are shown in Figures 3 and 4 for the first and second stages, respectively. Because of the severity of the environment in which each blade is subjected, a variety of causes have emerged including high cycle fatigue (HCF), low cycle fatigue (LCF), hydrogen environment embrittlement (HEE), and combinations of the above.

At the onset of the blade analysis effort, it was determined that the pressure side fir tree transverse lobe cracks (Fig. 3-h) on the first stage and the transverse downstream fir tree face/corner cracks (Fig. 4-f) on the second stage were the most critical, and should be analytically assessed. The criticality of these two crack occurrences stemmed from the fact that their continued growth could result in a potentially catastrophic event. The first stage cracks, although with a low frequency of occurrence, had accumulated fairly large depths on several blades (Fig. 5). This gave substance to the possibility of a complete fir tree neck 1 or neck 2 failure, which would greatly increase the loads on the remaining two lobes. The second-stage cracks also appeared infrequently, but one blade from HPFTP 0407 gave considerable concern because of a single large through crack 0.160 in. deep after only eight engine test cycles (Fig. 6).

Post test inspection of both fir tree crack types described above revealed that their origin was predominantly from hydrogen-assisted low-cycle fatigue initiated during the first mainstage engine cycle and grown in subsequent cycles. A detailed review of the first-stage blade cracks indicated transgranular fracture initiating at surface carbides and porosity regions propagating as a function of strain level. Similar investigations of the second-stage downstream fir tree face cracks pointed to crystallographic fracture also initiating at carbides on the surface. The second stage downstream fir tree corner cracks proved to be crystallographic fracture independent of surface carbides with secondary initiation due to high cycle fatigue. Subsequent plastic strain-to-crack initiation tests accomplished on the blade material MAR-M-246(Hf) DS (as ground) in 5000 psi hydrogen have indicated that in the room temperature region, cracking was very likely to occur with the onset of any plastic strain component. Some results of this testing are depicted in the bar chart shown in Figure 7. This figure also graphically depicts the fact that blade temperature is a factor in crack initiation, as well as the actual strain magnitude.

HIGH PRESSURE FUEL TURBOPUMP
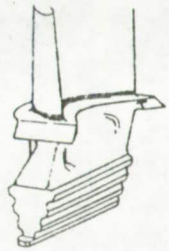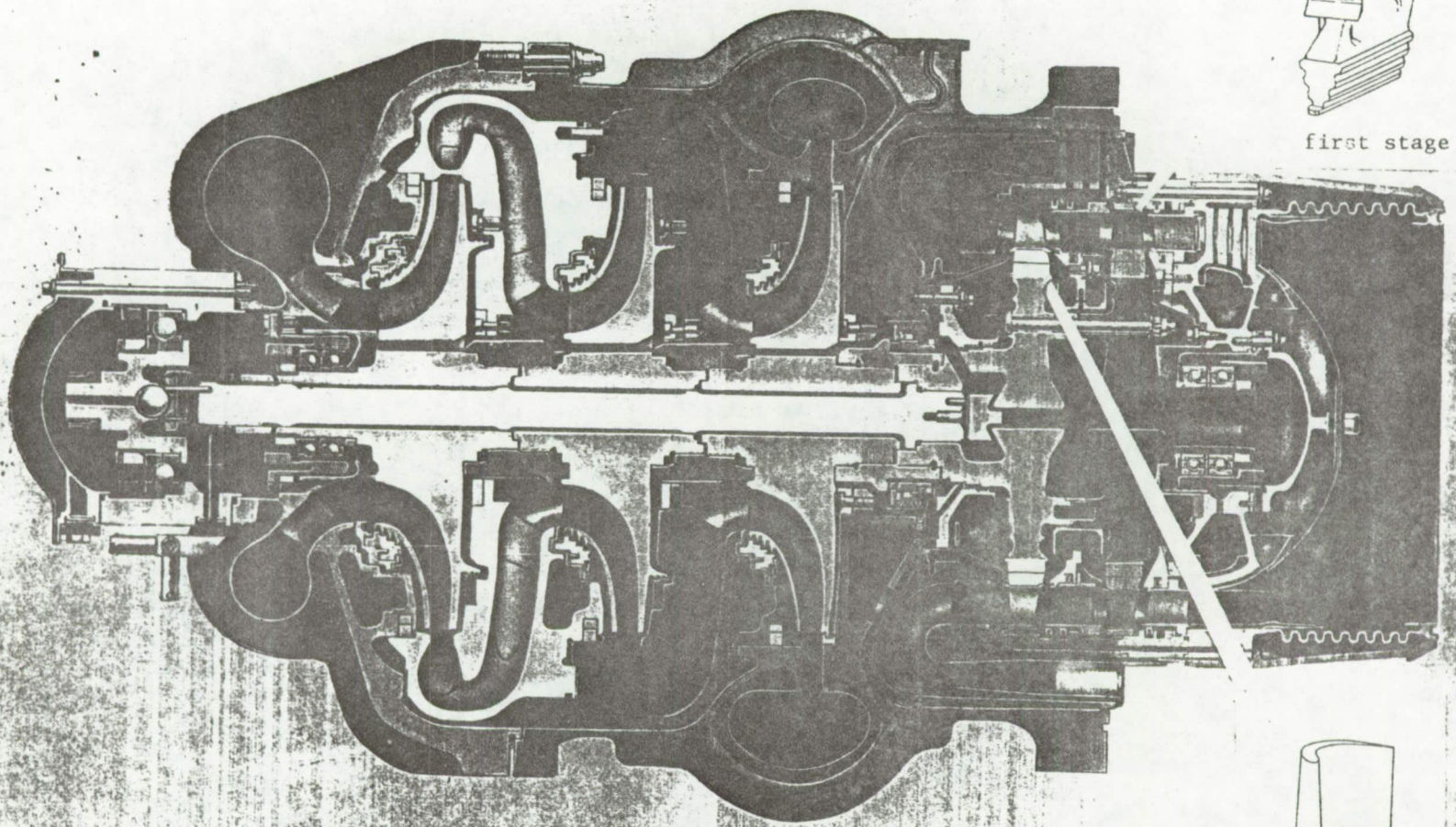
first stage
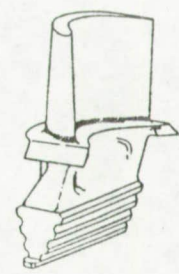
second stage

Figure 1. Fuel turbopump section.
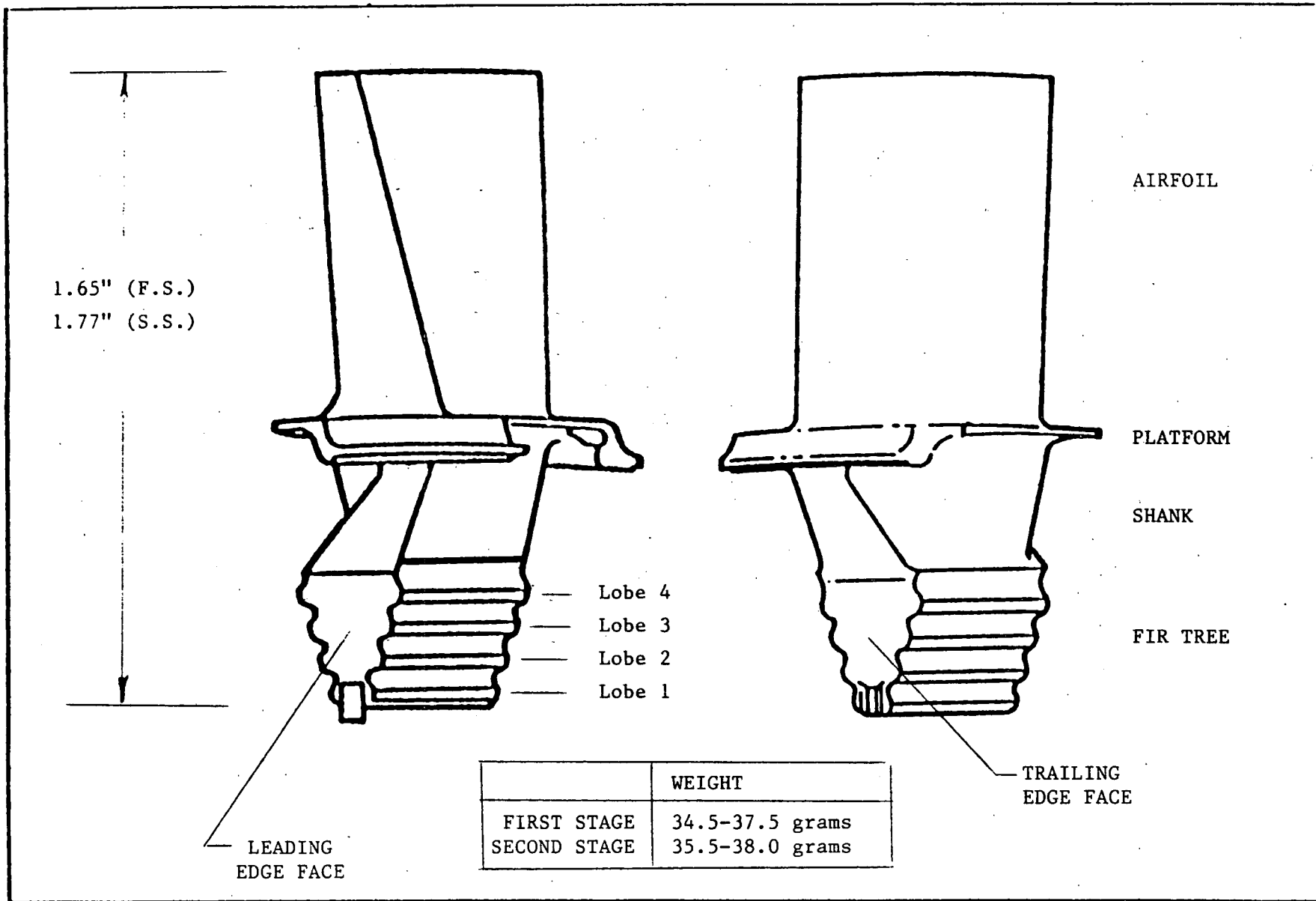
Figure 2. First- and second-stage blades.
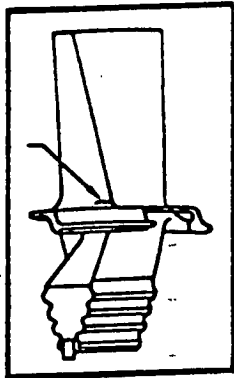
(a)
TRANSVERSE LEADING
EDGE AIRFOIL
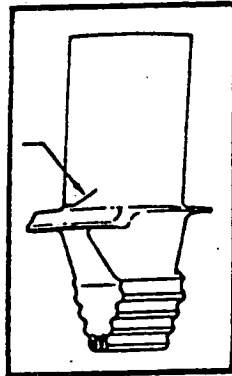
(b)
TRANSVERSE TRAILING
EDGE AIRFOIL
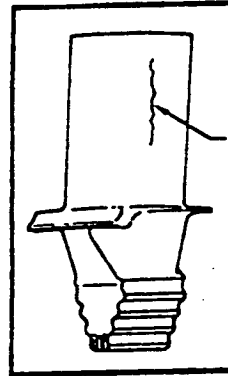
(c)
RADIAL AIRFOIL
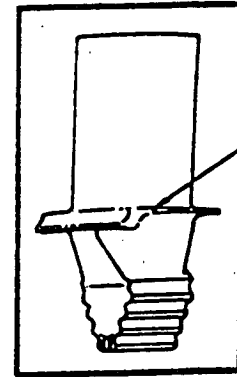
(d)
INTERGRANULAR AND INTER-
DENDRITIC (I_G/I_D) PLATFORM
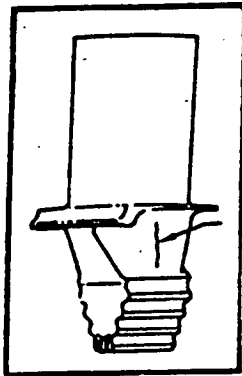
(e)
RADIAL SHANK
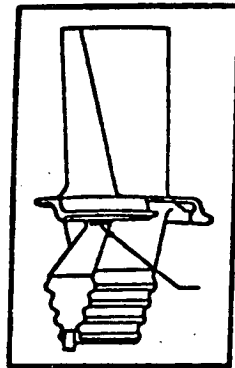
(f)
TRANSVERSE
UPSTREAM SHANK
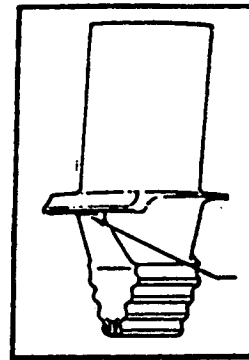
(g)
TRANSVERSE
DOWNSTREAM SHANK
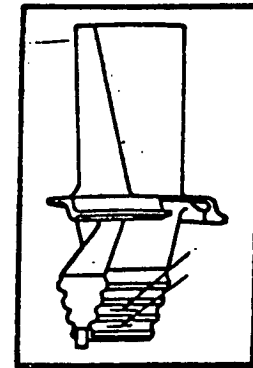
(h)
TRANSVERSE
FIRTREE LOBE

Figure 3. First-stage turbine blade cracks.
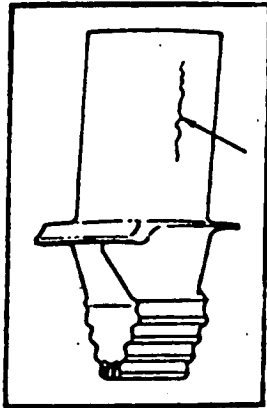
(a)
RADIAL AIRFOIL
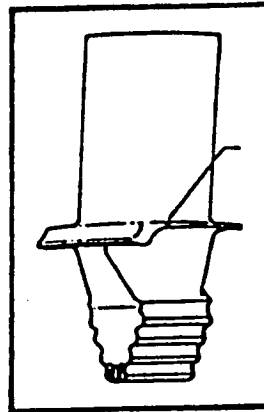
(b)
INTERGRANULAR AND INTER-
DENDRITIC (I_G/I_D) PLATFORM
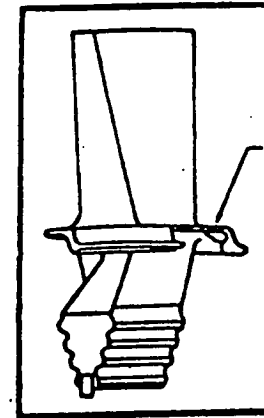
(c)
CRYSTALLOGRAPHIC
PLATFORM
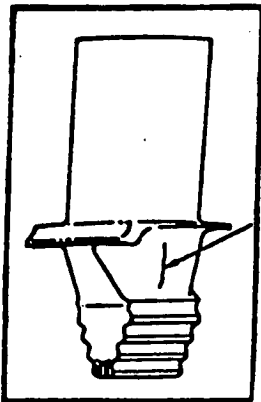
(d)
RADIAL SHANK
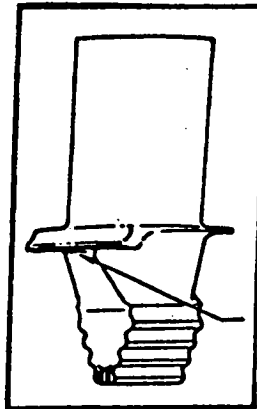
(e)
TRANSVERSE
DOWNSTREAM SHANK
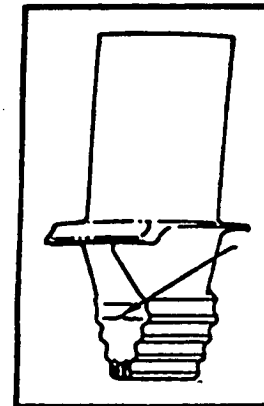
(f)
TRANSVERSE DOWNSTREAM
FIRTREE FACE

Figure 4.   Second-stage turbine blade cracks.

GROWTH MEASURED FROM PRESSURE SIDE, FIRTREE CENTER, 90° ANGLE THROUGH BLADE THICKNESS TO SUCTION SIDE

ACCUMULATED CRACK DEPTH (INCHES)

.130
.120
.110
.100
.090
.080
.070
.060
.050
.040
.030
.020
.010
0

0 2 4 6 8 10 12 14 16 18 20

ARREST LINES
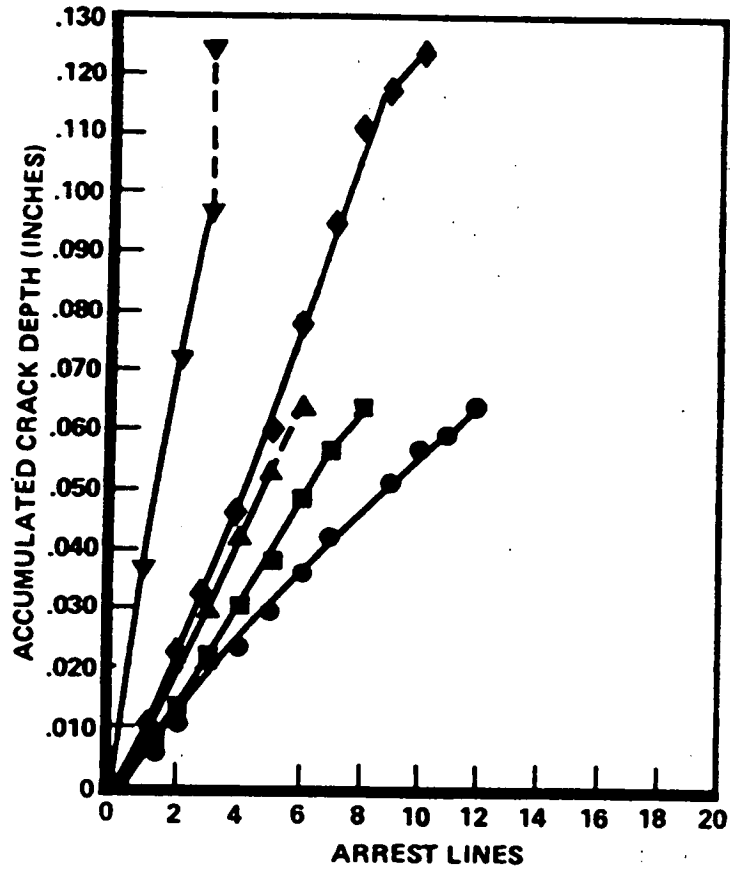
S/N	U/N	LOBE
◆ CQ22	9509	2
▼ R512	9410	2
▲ R53	2017R2	1
■ AP029	5102R1	1
● FR7	4104R1	1

2nd LOBE
1st LOBE
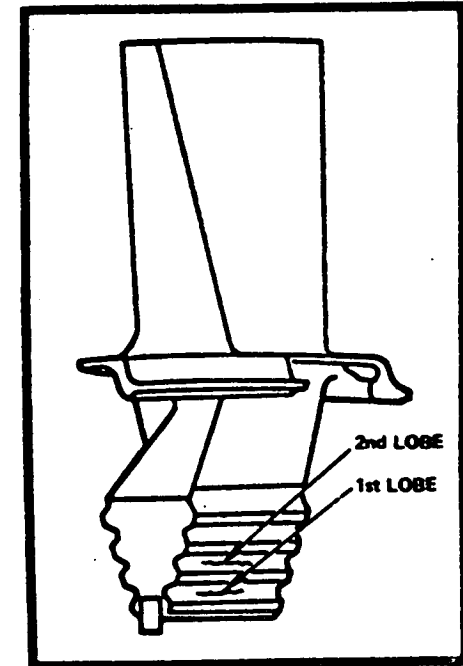
63 BLADES PER SET

(REFERENCE 1)

Figure 5. First-stage fir tree lobe crack growth.

ACCUMULATED CRACK DEPTH (INCHES)

ARREST LINES

S/N	U/N	
◆ CQ22	9509	
▼ R512	9410	
▲ R53	2017R2	LOBE CRACKS
■ AP029	5102R1	
● FR7	4104R1	
◇ N928	2414R1	
▽ HG027	5102R1	FACE CRACKS
△ GR030	4104R1	
□ FM011	4104R1	

COMPOSITE PLOT OF CRACK
GROWTH RATES FOR FIRST
(LOBE) AND SECOND (FACE)
STAGE HPFTP FIR TREE
CRACKING (NOTE: ALL MEASURE-
MENTS REPRESENT TRACES ORIENTED
IN THE SAME DIRECTION, 90° TO
THE LOBE OR FACE HORIZONTAL)

DOWNSTREAM
FACE

59 BLADES PER SET

(REFERENCE 1)

Figure 6. Second-stage downstream face crack growth.

MAR—M246, AS—GROUND, 5000psi H$_2$
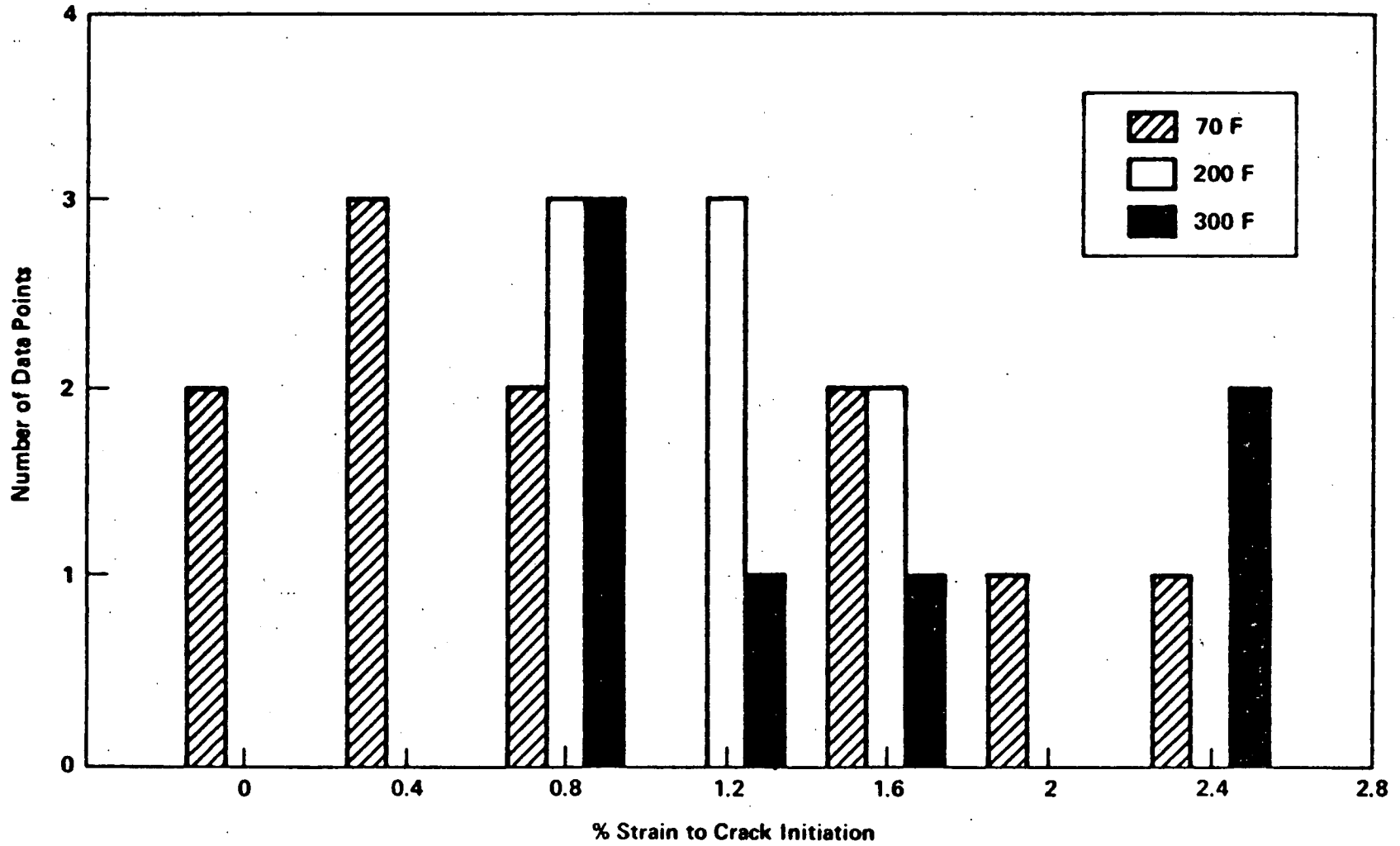
Figure 7. MAR-M-246 plastic strain to crack initiation.

Since the mode of crack initiation has been established as hydrogen assisted low cycle fatigue, the proper conditions including strain level, temperature, and the presence of hydrogen must therefore all occur simultaneously. The only opportunity for this to happen below the platform in the fir tree area is during the steady-state mainstage portion of the engine firing. The other two conditions in the firing sequence are the start-up and shut-down transients, where all the pertinent load factors are not present at the same time. The baseline environment chosen for the ensuing analysis was the full power level (FPL-109%) steady-state condition. This phase of the engine operation represents the period of performance when all engine parameters such as speed, pressure, coolant flow, temperature, and thrust have stabilized.

The commitment to embark on such a complex analytical problem was reinforced by the criticality and the potentially destructive effects that continued growth in these two specific turbine blade cracks could produce.

MODEL DEVELOPMENT

The primary goal of the analysis was to create finite element models of the first- and second-stage SSME HPFTP turbine blades and rotors that would include sufficient analytical accuracy to confidently predict the strain state existing throughout the fir tree. Because of the geometric and environmental complexity of these turbine components, 3D models were seen to be the only tool fully capable of producing accurate results. Three-dimensional analytical tools require a lot of development time and generally yield an overwhelming amount of output that also require a great deal of manpower for assessment. With this in mind, 2D and 3D models were begun simultaneously. These less complex 2D models provide a baseline analysis from which the 3D models can be more easily appraised. Another good reason for 2D development is that they can be efficiently utilized in parametric studies. These 2D and 3D models were all executed on the MSFC Cray X-MP/44 computer system.

Two-Dimensional Model (2D)

The 2D nodal point locations were actually generated manually so that a high degree of accuracy could be obtained in the fir tree neck regions. Since this is a high stress concentration area, past experience has shown a need for 10 to 12 elements along the perimeter of the neck. Another guiding factor was to create only four sided elements (quadrilaterals) and to maintain a reasonable orthogonal relationship between the sides in the highly stressed portion of the model. Both blade and rotor models were developed and checked out on the MSFC Intergraph IGDS CAD/CAM system and translated into the ANSYS structural program. Figure 8 shows a plot of the 2D fir tree part of the model. Note the higher concentration of elements in the neck regions. The total model (Fig. 9) consisted of 1541 isoparametric plane strain elements in the rotor, and 40 bi-linear connecting gap elements. Since there are 63 first-stage blades and 59 second-stage blades, the rotor models were represented by 1/63 (5.71428 deg arc) and 1/59 (6.10169 deg arc) of each rotor, respectively.

Determination of the blade mass to be used in analysis was accomplished first by reviewing the measured mass of every first- and second-stage blade on five assembled turbopumps.
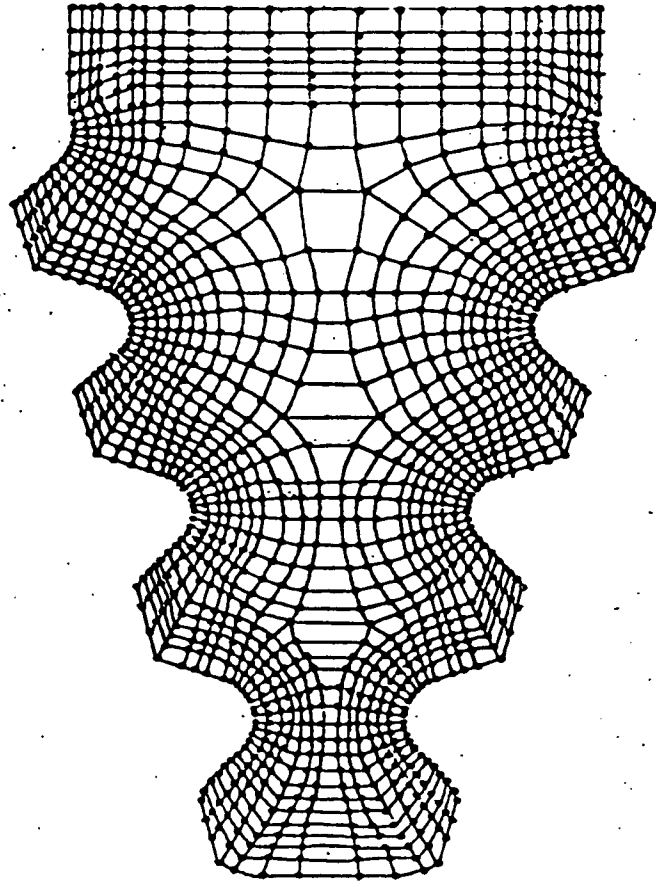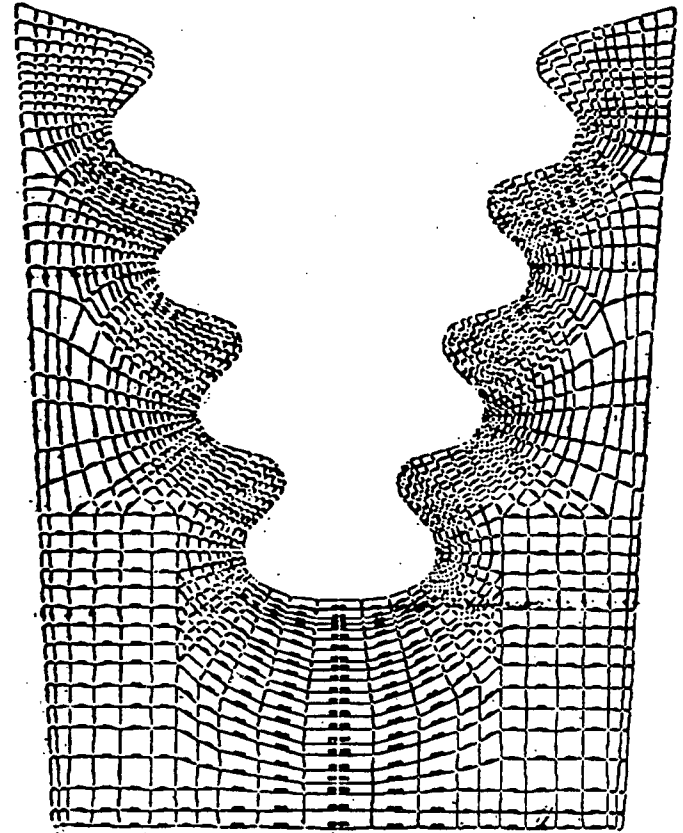
BLADE   ROTOR

Figure 8.   HPFTP 2D fir tree model.
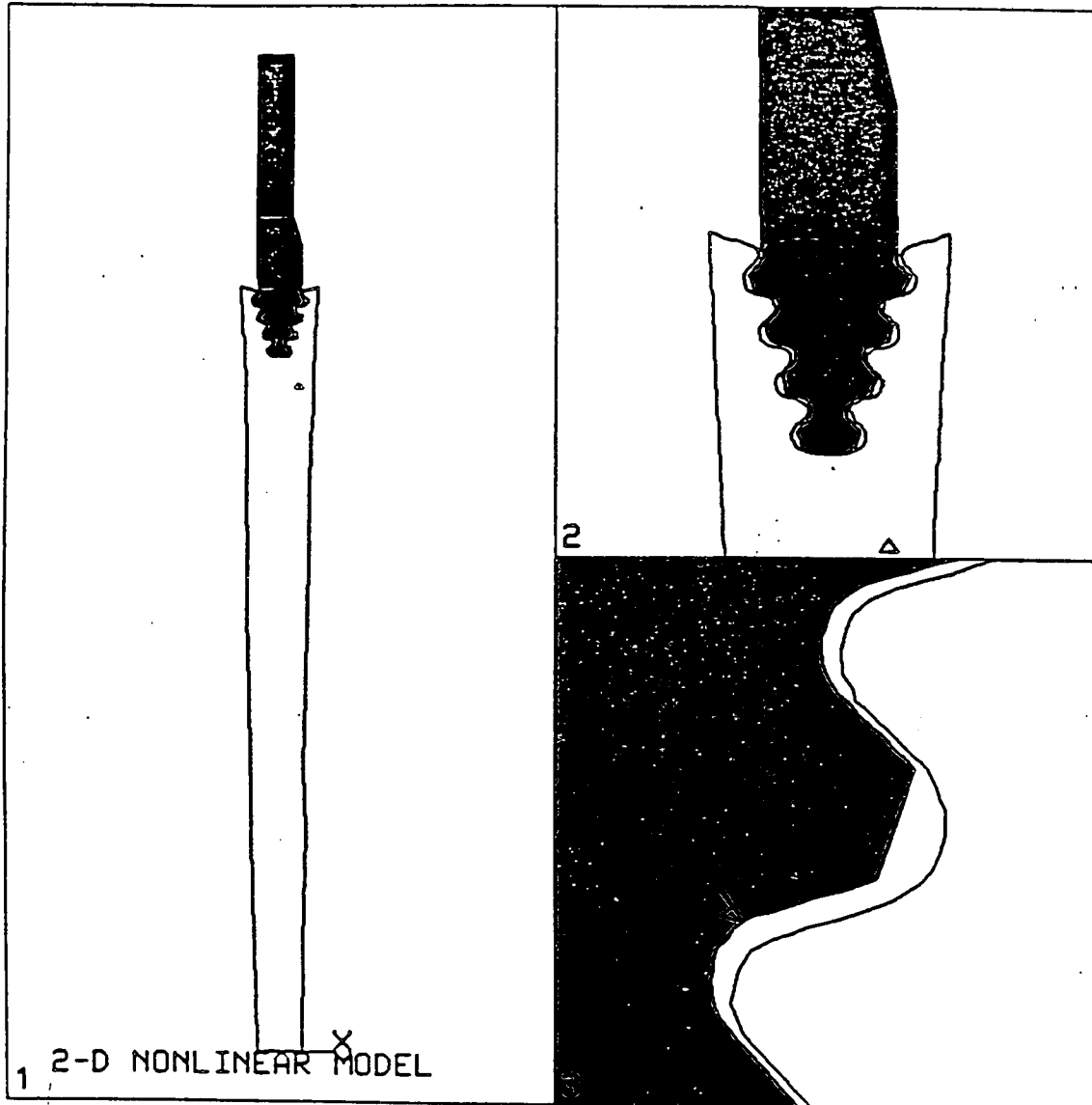
ANSYS 4.2
JUL 29 1987
16:44:27
PLOT NO.   2
PREP7 ELEMENTS
MNUM=1

ZOOM
ZV=1
* DIST=3.02
* XF=.00323
* YF=2.75
EDGE

WIND=2
ZOOM
ZV=1
* DIST=.484
* XF=.00323
* YF=4.14
EDGE

WIND=3
ZOOM
ZV=1
* DIST=.0726
* XF=.0939
* YF=4.05
EDGE

ORIGINAL PAGE
COLOR PHOTOGRAPH

2-D NONLINEAR MODEL

Figure 9.   HPFTP 2D blade/fir tree disk model.

The design tolerance is 34.5 grams (g) to 37.5 g (0.076 to 0.082 lb) for the first stage, and 35.5 g to 38.0 g (0.078 to 0.083 lb) for the second stage. Results of the measured mass data indicated a fair number of blades on both stages were near the upper end of the specification. Therefore, for all 2D and 3D analyses, the maximum blade mass was used. From previously developed blade profile models, the center of gravity (C.G.) was determined and is shown in Table 1 (also Fig. 10).

TABLE 1.   2D MODEL WEIGHT/CENTER OF GRAVITY

	First Stage	Second Stage
Weight	0.082 lbs	0.083 lb
Rcg	4.5399 in.	4.5162 in.
Xcg	-0.0166 in.	-0.0162 in.

Note that the 2D model represents a section through the C.G. of the blade with the plane perpendicular to the side of the fir tree. This side canted 19 deg off the global X-axis.
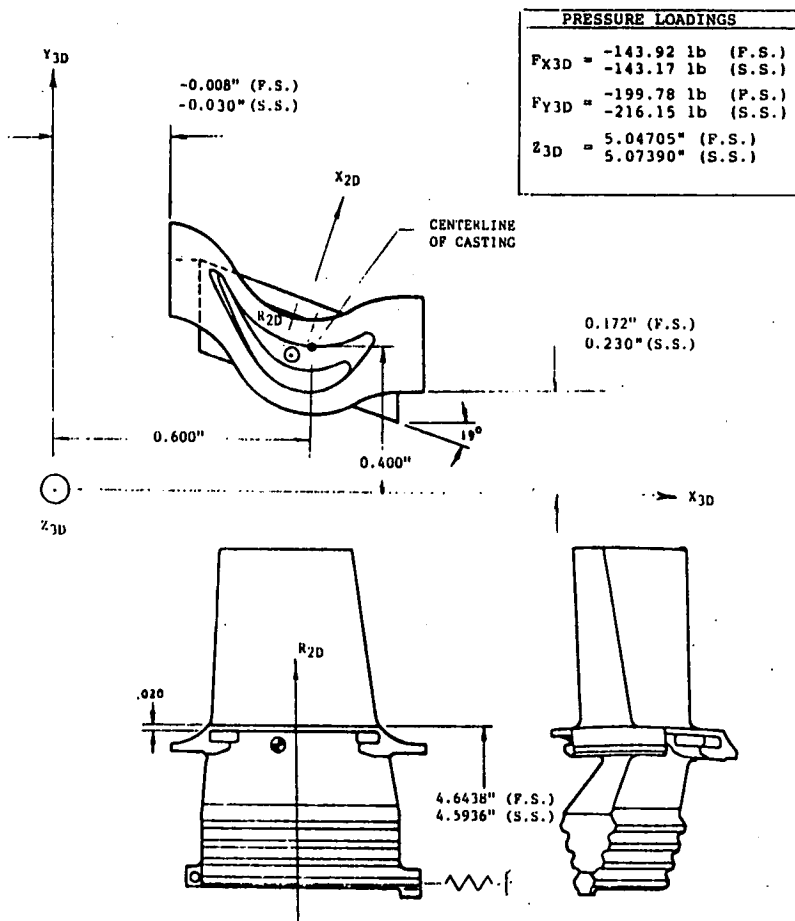
Figure 10.   HPFTP turbine blade coordinate systems.

Three-Dimensional Model (3D)

Development of the 3D model was begun with the use of existing first- and second-stage platform/airfoil models [3]. This then left the fir tree and a transition zone between the fir tree and shank. Since the cracking problems were centered around the fir tree, building of this region was gone about in a careful, systematic manner. The ideal approach would have been to simply take the previously generated 2D fir tree nodal scheme and reproduce it until the desired 3D model emerged. This, however, proved to be far too large a problem for practical, timely results. To arrive at an acceptable element arrangement, five models of increasing element density were constructed and subjected to various loading conditions. These loadings were utilized in assessing the resultant stress concentrations that were produced on each. One such case, shown in Figure 11, depicts the stress concentration (Kt) versus model complexity for a uniform radial load across the top of the fir tree. The more refined the model, the more the Kt approached the value generated by the 2D model. The actual 3D model arrangement used, as shown in Figure 12, was a model whose element configuration was between scheme 3 and 4 (Fig. 10). This model yielded Kt magnitudes within 8 percent of the baseline 2D model predictions.

It was decided early on that the basic fir tree 3D model definition would be used on both first and second stages. The only difference being that the second stage was some 0.030 in. longer. Accuracy was required not only in the neck region but also on the face of the fir tree. Hence, each fir tree face contained 400 brick elements. To keep the aspect ratio less than 5.0, a total of 30 such layers were generated again by the MSFC CAD/CAM system and translated into the ANSYS structural program. Results of this enormous task produced very large finite element representations as shown in Table 2.

Figure 13 is a plot of a blade model sitting in a symmetrically generated rotor model. Figure 14 shows the actual graphics image of a blade attached to a "slice" of the rotor. This "slice" represents 1/63 (5.71428 deg arc) of a first-stage rotor and 1/59 (6.10169 deg arc) of a second-stage rotor. The actual rotor "slice" is canted at 19 deg to the pump centerline (global X-axis). Figures 15 and 16 depict closeup views of the blade model, revealing details of the airfoil, platform, fir tree, and upper rotor.

Again the blade models for both stages employed the largest acceptable mass. The weight and center of gravity (C.G.) of each blade is shown in Table 3.

MATERIAL MODEL

In any structural analysis, a key parameter in producing reliable results is the determination of material properties. The MSFC Materials and Processes Laboratory (EH) surveyed the available data and developed the required properties [6,7]. The HPFTP turbine blades are a cast nickel base alloy MAR-M-246(Hf) DS material. The alloy is directionally solidified (DS) which is a casting method of producing long axial grain boundaires and a minimum of transverse grain boundaries. With directional solidification, different properties are developed in the direction of solidification (longitudinal direction) than in the orthogonal plane (transverse direction). Table 5 lists the linear-orthotropic mechanical properties versus temperature utilized in the analyses. These values were predominantly used in 3D analytical efforts.

NECK 3 STRESS CONCENTRATION

◇————◇ RESTRAINED ISOTROPIC   #————# UNRESTRAINED ISOTROPIC

X————X RESTRAINED ORTHOTROPIC   ☐————☐ UNRESTRAINED ORTHOTROPIC
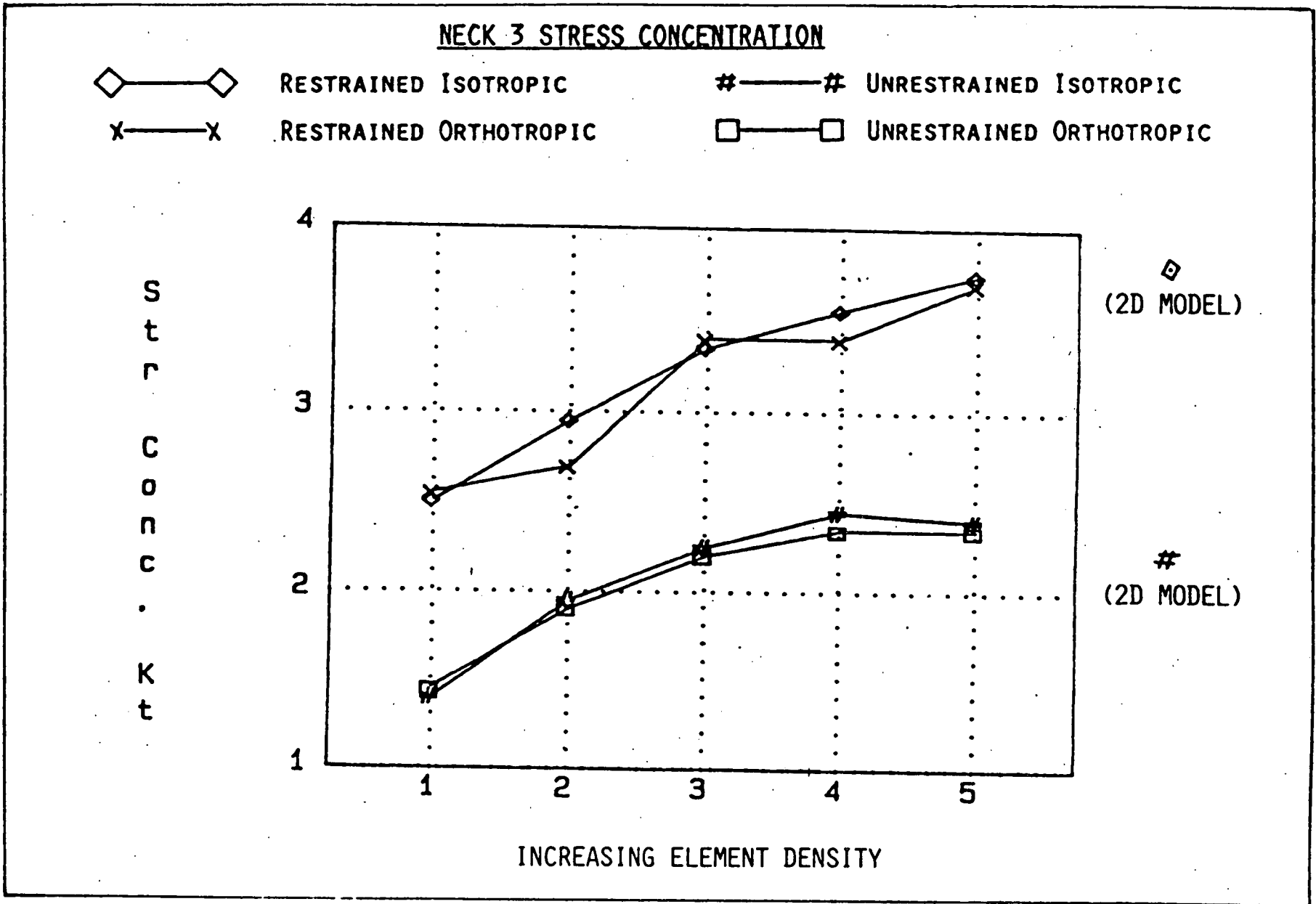
Figure 11.   Stress concentration versus model complexity.

ELEMENT DENSITY IN FIRTREE AREA
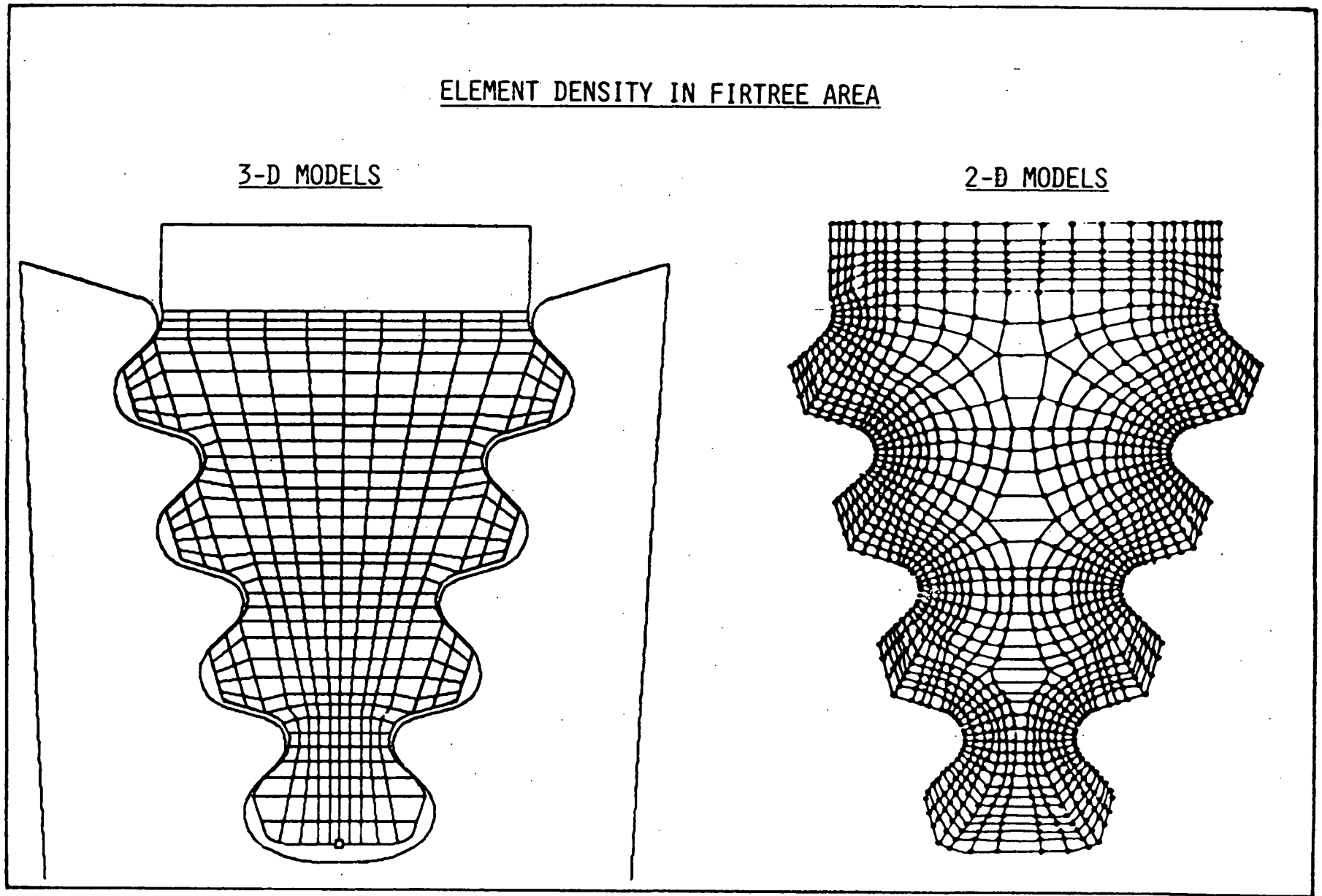
3-D MODELS

2-D MODELS

Figure 12.   2D and 3D fir tree element density.

TABLE 2. 3D MODEL NODES/ELEMENTS

	Nodes	Isoparametric Elements	Bi-Linear Gap Elements
First Stage Blade	17495	15086	
First Stage Rotor	12308	9767	744
Second Stage Blade	16822	14476	
Second Stage Rotor	12350	9770	744

TABLE 3. 3D MODEL WEIGHT/CENTER OF GRAVITY

	First Stage	Second Stage
Weight	0.082 lbs	0.083 lbs
Xcg	0.58694 in.	0.58697 in.
Ycg	0.38717 in.	0.38771 in.
Zcg	4.5399 in.	4.5162 in.

TABLE 4. HPFTP ENVIRONMENT STATIONS

Location	Description	Radius (in.)
1	Upstream shaft core	0.125
2	Inner wheel cavity	1.20
3	Downstream shaft core	0.125
4	Forward cavity, inner	2.16
5	Foward cavity on disk	3.28
6	Forward cavity at fir tree	4.00
7	Forward cavity at shank	4.45
8	First stage nozzle	5.095
9	First stage airfoil	5.095
10	First stage shank	4.45
11	First stage fir tree	4.00
12	Mid cavity at first stage shank	4.45
13	Mid cavity at first stage fir tree	4.00
14	Mid cavity on first stage disk	3.525
15	Mid cavity seal, first stage side	2.84
16	Mid cavity seal, second stage side	2.84
17	Mid cavity on second stage disk	3.525
18	Mid cavity on second stage fir tree	4.00
19	Mid cavity at second stage shank	4.45
20	Second stage nozzle	5.095
21	Second stage airfoil	5.095
22	Second stage shank	4.45
23	Second stage fir tree	4.00
24	Aft cavity at shank	4.45
25	Aft cavity at fir tree	4.00
26	Aft cavity on disk	3.28
27	Aft cavity at laby seal exit	2.16
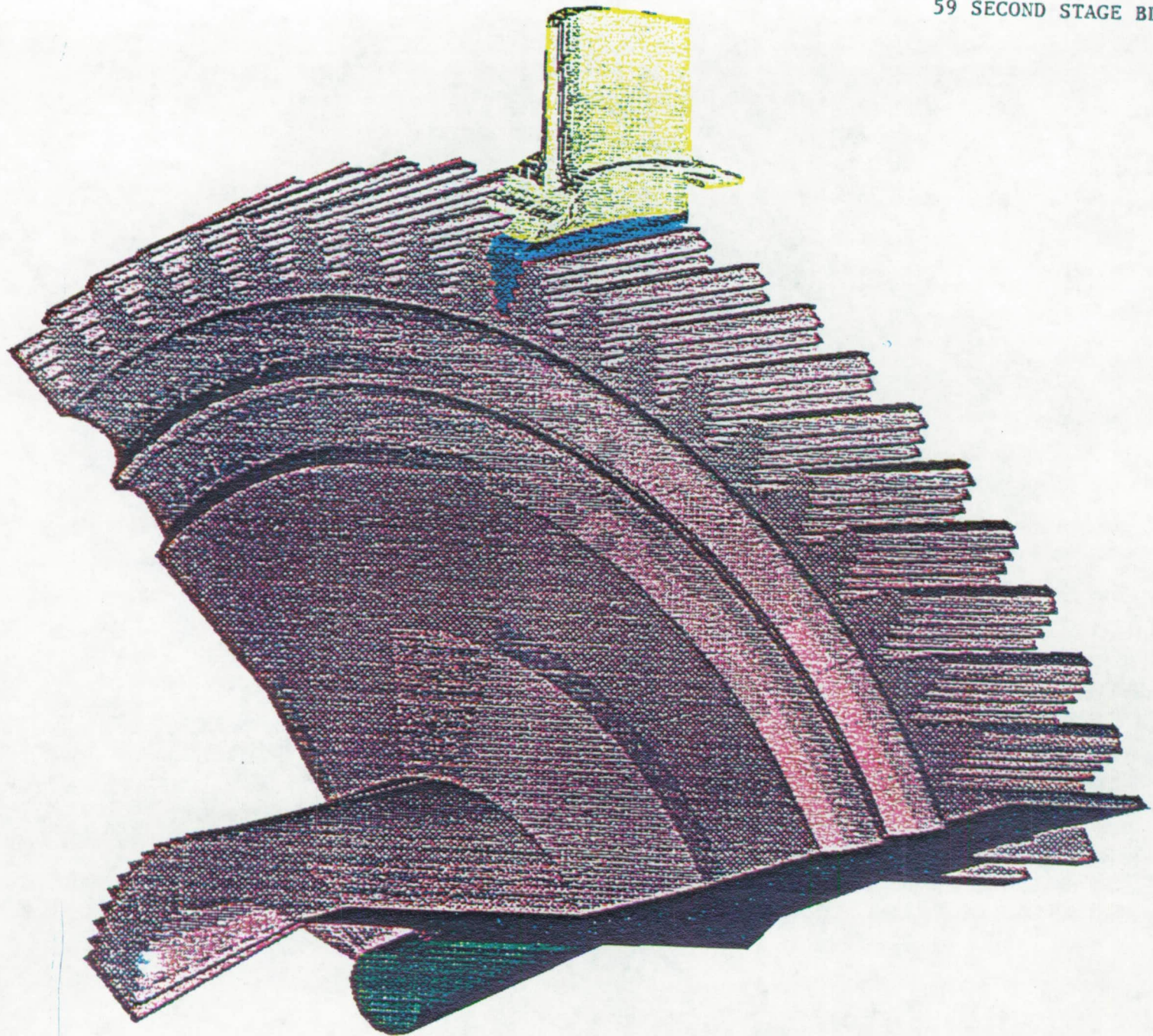
Figure 13. Blade with symmetrical rotor plot.
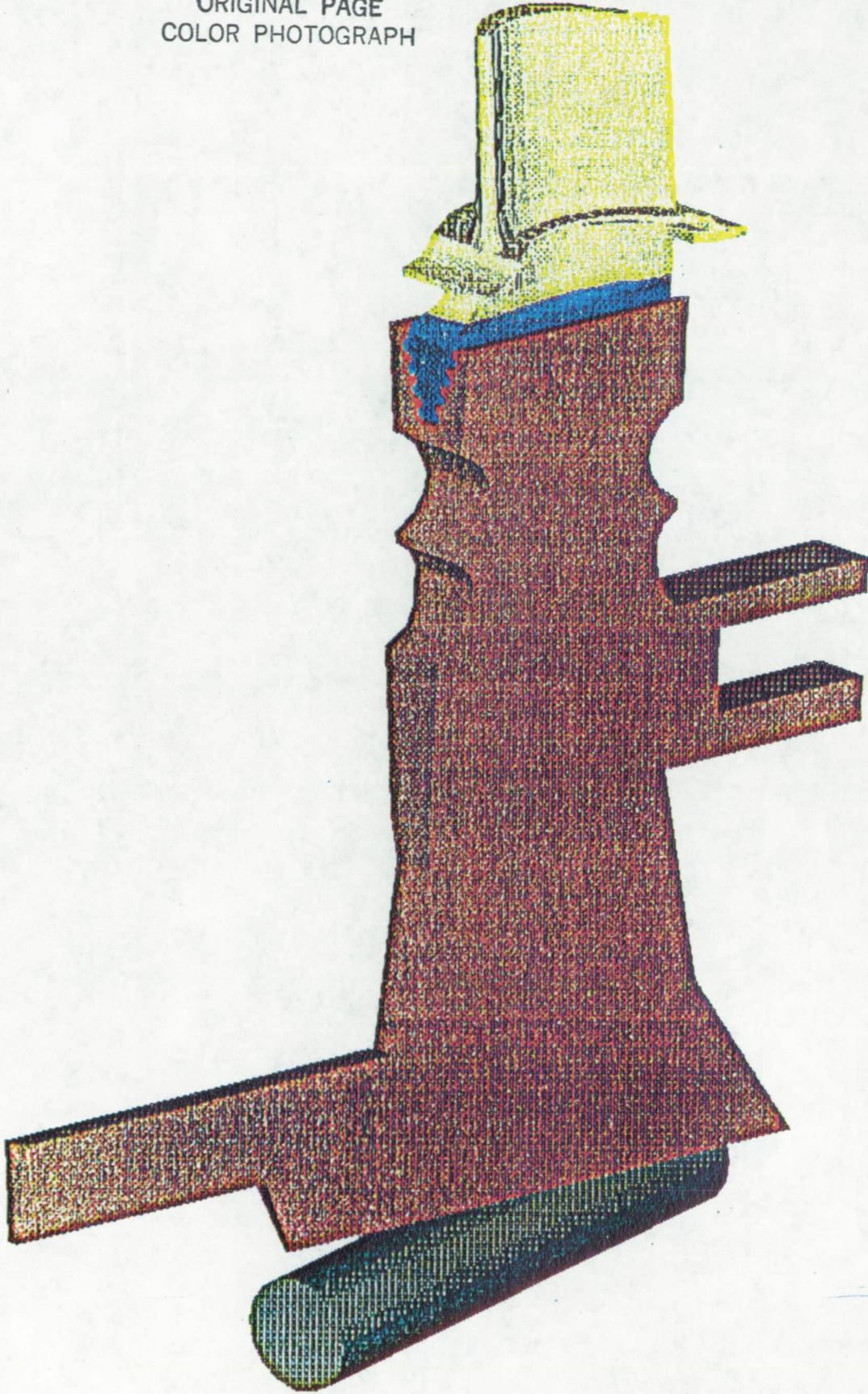
Figure 14. Blade and rotor model.
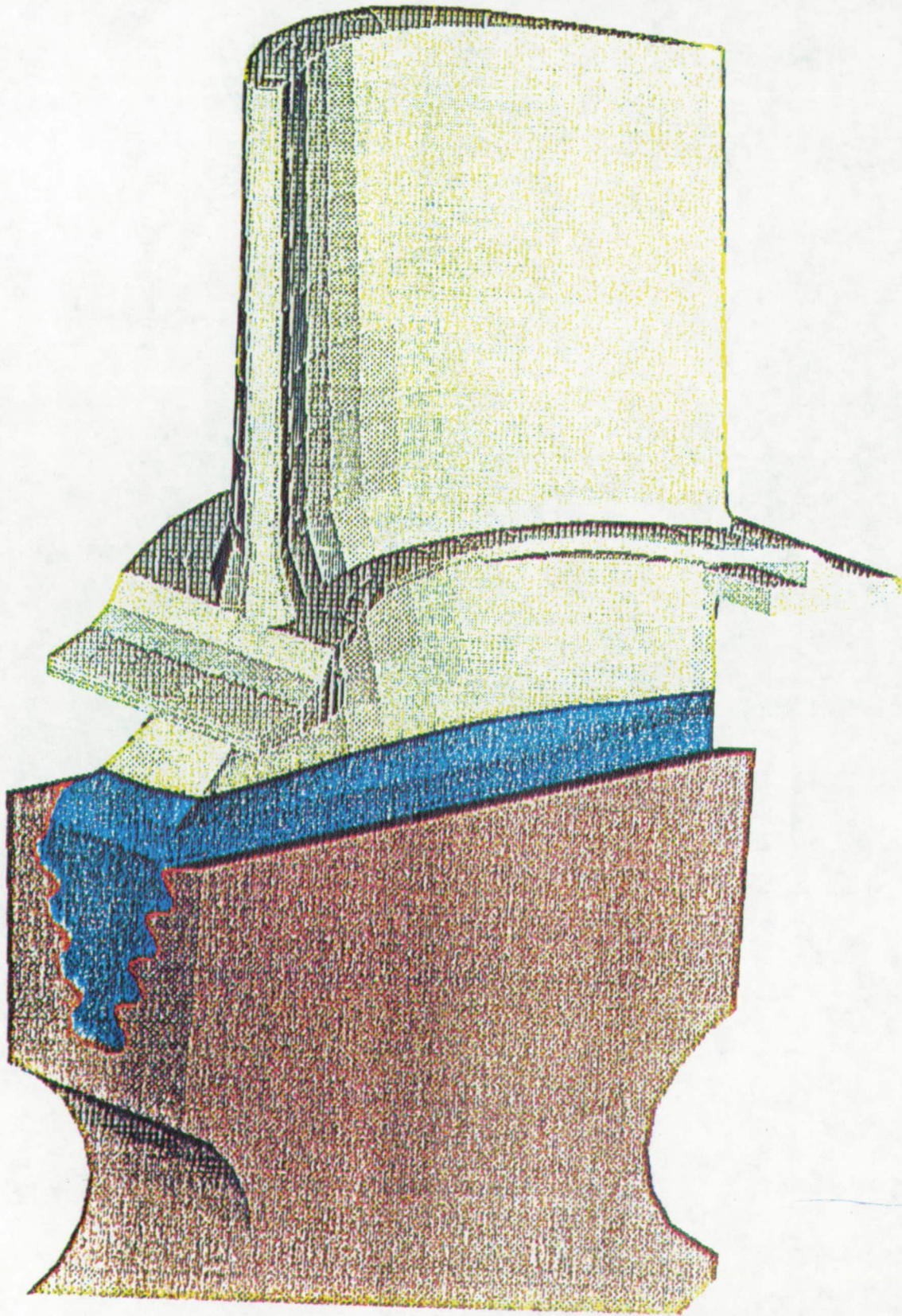
Figure 15. Blade/rotor attachment region.
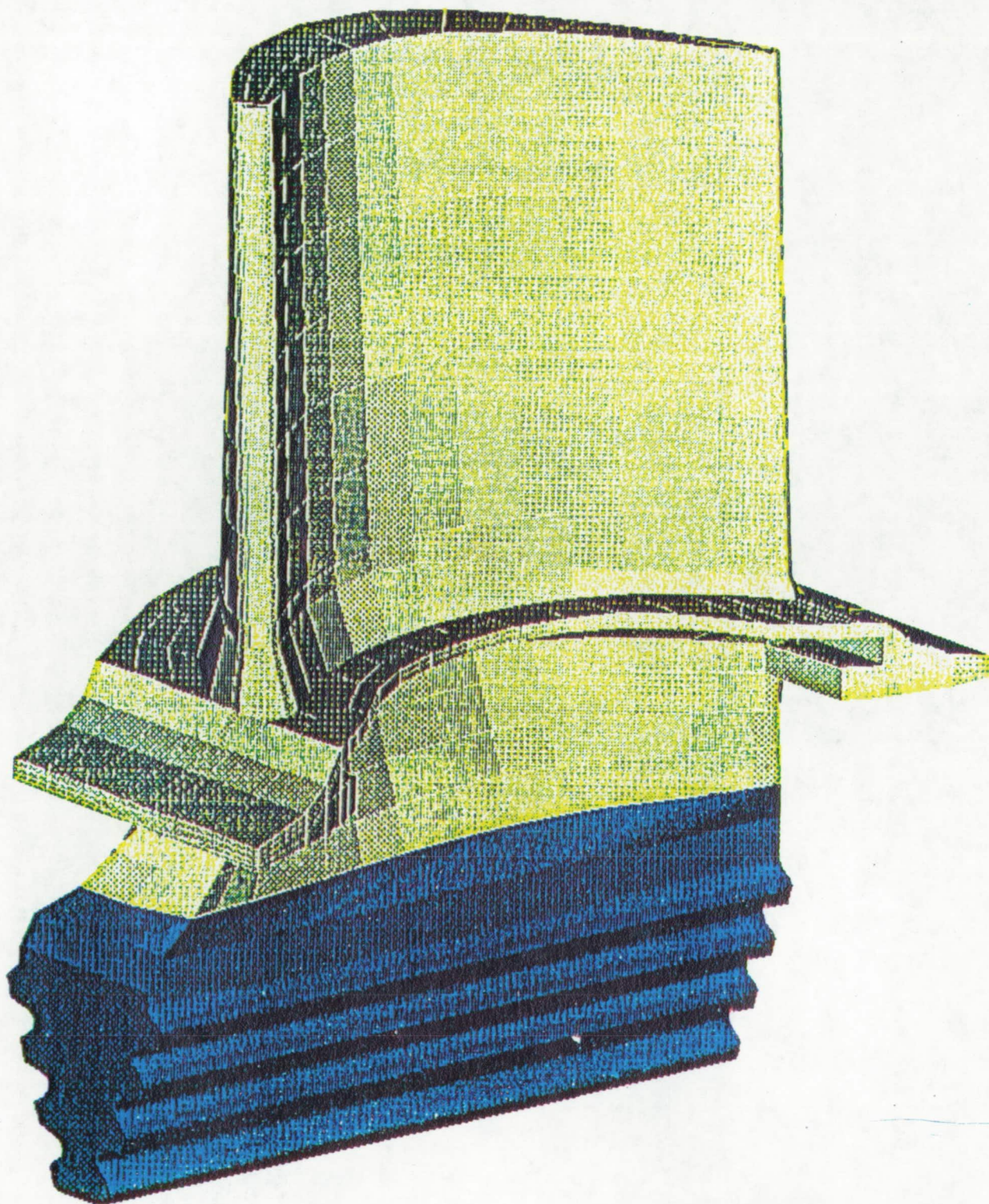
Figure 16.   Blade model.

TABLE 5. MAR-M-246 LINEAR-ORTHOTROPIC PROPERTIES

Temperature (°F)	EX EY (msi)	EZ (msi)	GXY (msi)	GYZ GXZ (msi)	NUXY NUYZ NUXZ	GTE micro-in./in./°F
-300	27.2	19.8	10.6	9.14	0.285	4.870
70	26.4	18.7	10.3	8.77	0.285	6.125
400	25.5	18.2	9.90	8.48	0.287	6.891
800	24.0	17.2	9.27	7.96	0.294	7.668
1300	22.1	15.7	8.39	7.17	0.317	8.393
1700	19.7	13.8	7.39	6.28	0.333	10.53

where

$$GXY = \frac{EX}{2(1+V)}$$

$$GYZ = GXZ = \frac{(EX+EZ)/2}{2(1+V)}$$

For the nonlinear portion of the analysis, stress-strain curves were input using a multilinear kinematic hardening model. The actual material response is represented in the ANSYS structural code by a set of von Mises yield criteria, each with an appropriate yield stress and weighting factor which are derived from the uniaxial stress-strain curves. Table 6 tabulates the stress-strain curve used for 2D analyses at room temperature.

TABLE 6. MAR-M-246 NONLINEAR STRESS-STRAIN CURVE

Point	Stress (ksi)	Strain (%)
1	80	0.4278
2	100	0.5978
3	107	0.6978
4	110	0.8278
5	120	3.8978

The HPFTP rotors are forged with Waspaloy material. Waspaloy is a vacuum-melted precipitation-hardened nickel base alloy which is strengthened by the precipitation of titanium and aluminum components and the solid solution strengthening effects of chromium, molybdenum, and cobalt. The mechanical properties of the alloy are depicted in Table 7.

TABLE 7. WASPALOY MATERIAL PROPERTIES

Point	Stress (ksi)	Strain (%)
1	124	0.4106
2	143	0.5106
3	155	0.7106
4	161	1.5106
5	173	3.9106

where:

E = 30.2 MSI

G = 11.6 MSI

V = 0.305

alpha = 6.4 E-06 in./in./°F

Linear elastic properties were used for all 3D efforts, while the nonlinear kinematic hardening material models were used exclusively in the 2D work.

ANALYSIS APPROACH

The primary tasks for the turbine blade analysis can be separated into three major categories as simulation, response, and life prediction. The simulation portion was concerned with the development of models for gasdynamics, thermal, and structural analyses. The response category concentrated on the implementation of these models to predict load conditions and associated stress/strain amplitudes. Finally, the life prediction activities resulted in the blade fatigue life evaluation.

A flow chart showing the major interfaces between analysis task areas is depicted in Figure 17. Figure 18 summarizes the analytical gasdynamics, thermal, and structural models used in the blade study. This report will, however, deal predominantly with the structural effort.

Gasdynamics

Analysis utilizing gasdynamics models was begun through the implementation of engine balance data as input into a one-dimensional turbine flow analysis of each of the two stages. The environmental data supplied from this task was taken from three sources [4] all at full power level (FPL-109%). Flow through the fir tree was determined from a computer code written at MSFC. Analysis of the aft-cavity was performed at MSFC using the PHOENICS computer code. Figure 19 shows a pictorial of the nodal breakdown in the aft cavity. Table 4 lists the description of each nodal location for this model. The remainder of the environmental data was taken from the
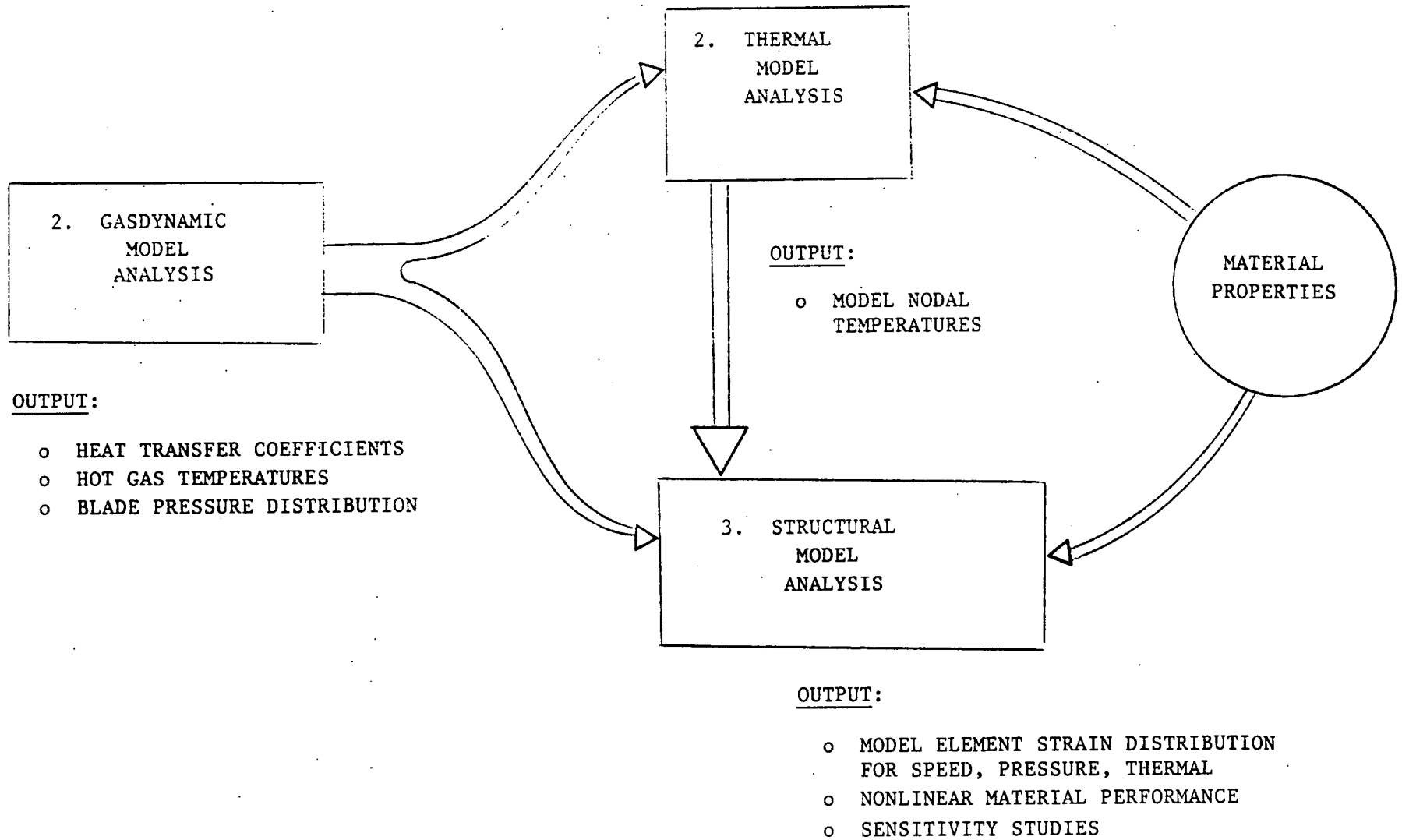
Figure 17. Model analysis flow.

o GASDYNAMIC FLOW MODELS

     - TURBINE 1-D FLOW
     - TURBINE COLLANT SYSTEM MODEL
     - NOZZLE/STRUT WAKE MODELS
     - MERIDL/TSONIC/BLAYER
       FLOW MODELS

o THERMAL MODELS

     - ANSYS 3D MODELS
     - SINDA MODEL

o STRUCTURAL MODELS

     - ANSYS 3D STRESS MODELS
     - ANSYS 2D STRESS MODELS
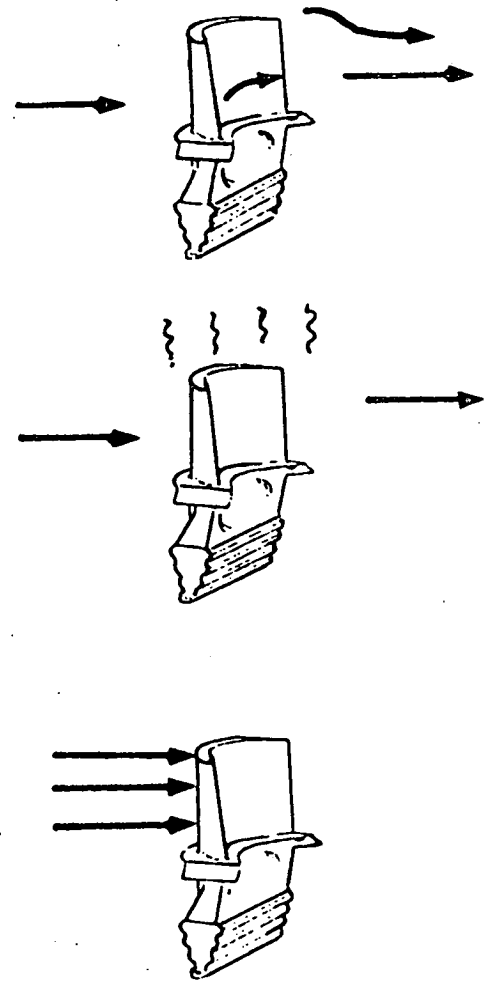
(REFERENCE 3)

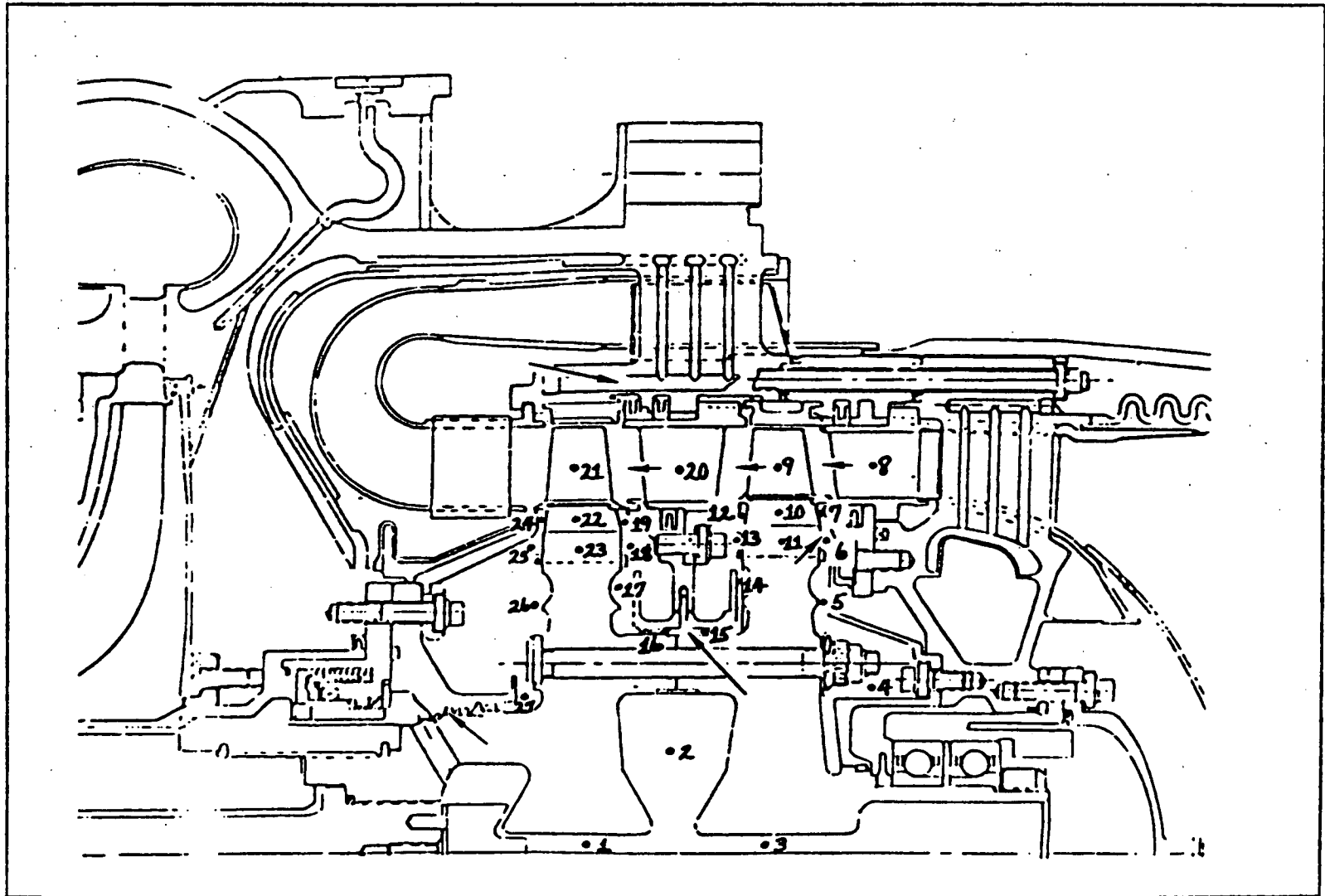Figure 18. Analytic model development.

Figure 19. Aft cavity model.

Lockheed HPFTP models [3] or was calculated from the available test data. Utilizing the 3D structural model node locations, the airfoil pressures were computationally calculated so that it was not necessary to perform any complex interpolation. This effort thus provided the pressure profile directly to the structural model for both first and second stage blades. These profiles were subsequently integrated across the entire airfoil areas with the resulting torque-producing component calculated. The first-stage rotor produced 63,523 in.-lb of torque, while the second-stage developed 64,706 in.-lb. The total turbine torque was therefore 128,229 in.-lb, with the engine balance data yielding 126,900 in.-lb. It can be seen that only a 1 percent error in overall torque is present from the gasdynamics analysis. In addition to the airfoil pressure profiles, the gasdynamics analysis developed hot gas temperatures, heat transfer coefficients throughout the blades, and other necessary boundary data for the planned steady-state thermal analyses.

Thermal

The full power level (FPL-109%) thermal analysis for both stages was accomplished by utilizing 3D structural ANSYS models along with the gasdynamics analysis input [5]. In addition, finite difference (SINDA) models were generated for comparison with ANSYS results. The ANSYS models yielded close agreement with the SINDA models in the fir tree area of both blades. By using the previously assembled ANSYS model as a thermal tool, the steady-state temperature profiles for both blades were again generated for each structural model node. This effort provided the thermal conditions without any interpolation or extrapolation of data, circumventing a good source of error.

Structural

With the gasdynamics and thermal analyses completed for both stages, the pressure and thermal profiles were available as direct input for the 2D and 3D models. The only remaining load component was that resulting from the steady-state centrifugal speed of the turbine. This was input by ANSYS automatically by calculating the mass and radius location of each element. The resulting force being the multiplication of mass times radius times the square of rotation rate.

Structural boundary conditions for the 2D models simply involved a symmetric boundary along both edges of the rotor "slices." Cyclic symmetry is appropriate here, but was not utilized because the symmetric analysis showed a negligible difference in the distribution of displacement from one side to the other. The only other boundary condition included the use of frictionless gap elements to transfer loads between the blade and rotor fir trees. All four fir tree lobe flats were assumed to be in contact prior to the full power level (FPL-109%) loading of the turbine. This constituted the "baseline" 2D analysis. The effects of non-uniform fir tree lobe contact (fit up tolerance) and of friction on the "baseline" cases are discussed later in this report. Initial checkout runs were made with the use of linear elastic material properties, however, all remaining analyses were accomplished with multilinear kinematic hardening properties.

The 3D model structural boundary conditions also involved a simple symmetric boundary along both planes of the rotor "slices." To prevent pump axis translation of the rotor, the curvic coupling structure was restrained axially. To limit the blade fir tree from excessive axial motion relative to the rotor fir tree, blade shear load was

carried out by utilizing an opposing force at the base of the blade fir tree underneath the leading edge surface. To account for any slight imbalance of resolving forces, a soft spring was attached in the same area (see Fig. 10). As with the 2D models, the 3D models used frictionless gap elements to transfer loads across all four fir tree lobe flats of the blade and rotor. The full power level (FPL-109%) loading is considered to be the 3D "baseline" analysis.

In the case of the 3D solutions, the entire blade/rotor model could not be executed at one time. The primary roadblocks to a complete blade/rotor analysis were the limitations in core memory (4 meg. words) of the Cray X-MP/44 at MSFC, and the limitations of the wavefront solution size (3000 DOF) in ANSYS. Even by going to a substructured rotor approach, the Cray limitation remained an impossible hurdle. Giving up gap elements between the blade and rotor, which would reduce the wavefront size, was not considered an option since a minimum acceptable number had already been selected. The technique finally utilized was one that took the substructured rotor and calculated the effective rotor stiffnesses at each gap element, then assigned these stiffness magnitudes to the gap elements themselves. The actual procedure for doing this is shown in the Appendix.

Because of the complexity and size of the 3D tools, only linear elastic isotropic and orthotropic material properties were used in these analyses. This proved not to be a problem since small magnitudes of plasticity were present. Another positive factor for accepting a linear elastic 3D analysis is the fact that the build procedure for the blades has now been altered to include shot peening of the entire fir tree on both stages.

FIT-UP TOLERANCE STUDY

The 2D models were used to develop fit-up tolerance studies. The HPFTP turbine blades, as seen in Figure 10, have a four lobe fir tree configuration. Because of the physical size of the fir tree, fit-up is a critical issue in the development of a relatively uniform load distribution across this component. To gain some understanding into the effect of fit-up on the magnitude of strain occurring in the first stage fir tree neck, contact was assured on a neck with a varying gap on the remaining three lobe flats. This procedure was repeated several times and the resulting neck strains recorded. Figure 20 shows a plot of the percent change in neck 1 and 2 strains versus the gap on the three remaining flats. Clearly indicated by the study is the fact that a 30 to 35 percent increase can be readily seen with just a 0.00025 in. fit-up gap. This very significant potential strain change could in itself explain the reason for such a low frequency of crack occurrences in the first-stage fir tree necks. To reduce the possibility of such off-nominal strain excursions, some blade/rotor assembly procedures have now been altered. One such modification includes a reverse broaching of the gold-plated Waspaloy rotor. When similar studies were performed on the second stage fir tree neck 3 and downstream face, only a 10 to 15 percent increase in strain resulted. Thus, the fit-up parameter does not appear to be a highly significant one for second stage downstream face/corner cracking problems.

Neck 1&2 Strain vs. Gap at Remaining Three Flats

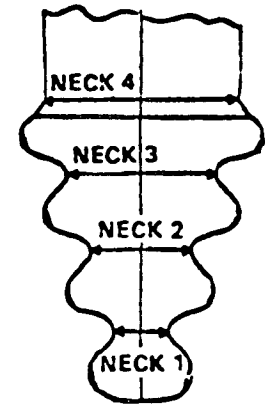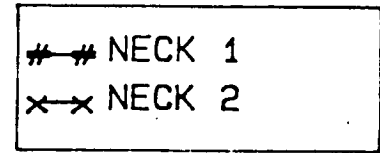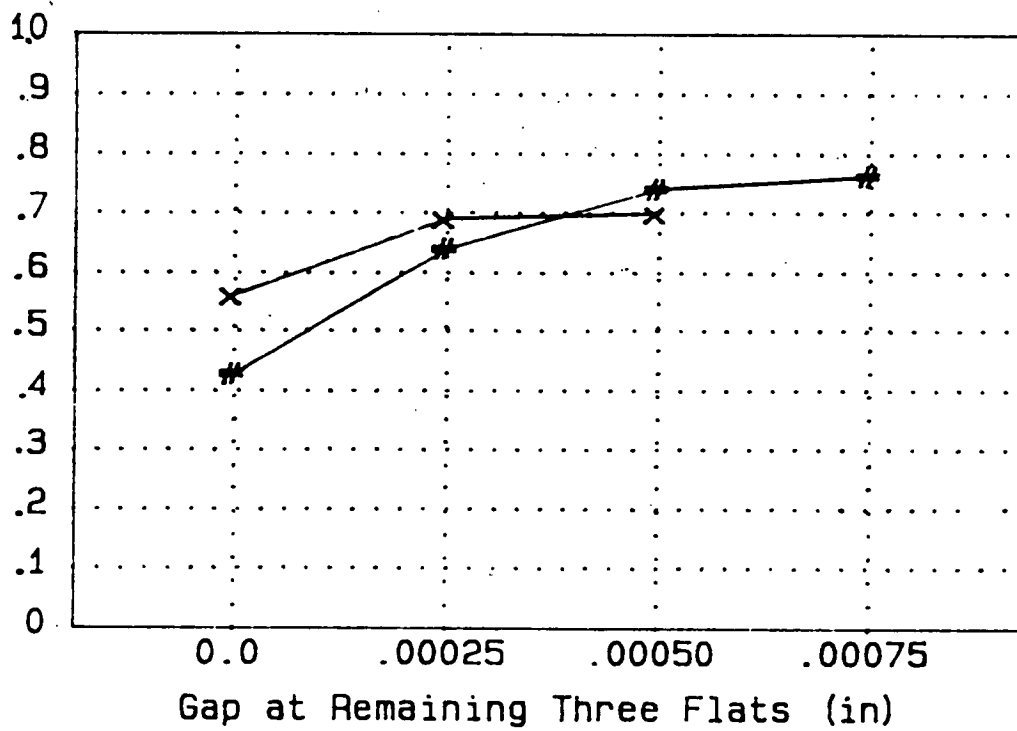

Figure 20. Fit-up tolerance study.

EFFECT OF FRICTION

As mentioned previously in this report, the blade loads for both 2D and 3D models were transferred into the rotor by frictionless gap elements. However, coefficient of friction (C.O.F.) tests accomplished between MAR-M-246 and Waspaloy indicated a range of values between 0.05 and 0.10. Utilizing the maximum test derived C.O.F., the 2D model gap elements were altered so as to develop shear forces between blade and rotor fir tree lobe flats. Results of the friction runs indicated that a 10 percent increase in neck strains could be expected in any of the four fir tree necks when using a 0.10 C.O.F. No 3D friction analyses have yet been run.

Another potential source of increased neck strain (especially in neck 1) related to friction, occurs if the turbine blade initially cocks over when first struck by the 5000 psi preburner hot gas. As the rotational speed increases, the blade will attempt to move to the upright frictionless position. If friction forces are introduced, additional rotationally induced strains may appear because the blade center of gravity has been moved slightly toward the suction side. This effect is presently being studied and may yield slightly higher strain increases than the 10 percent reported above.

STRAIN STATE AND LIFE

In general, components for calculating the principal strain magnitude were retrieved from both 2D and 3D analyses for post processing. In the case of the nonlinear material property 2D runs, the elastic and plastic strain components were actually extracted from the elements and post processed for the desired strain parameter.

Because the 3D models all used linear elastic materials, only elastic strain components applied. As with all isoparametric element formulations, actual strain data only mathematically appears at integration points. To obtain estimates of the surface strains it was necessary to use the ANSYS developed technique for recovery of such data. The nodal strains are arrived at by first computing the strains at the integration points closest to the nodes and then to extrapolating those results out to the nodes. This extrapolation is done using a bilinear or trilinear least squares curve fitting procedure. For plotting, the nodal strains are then averaged to yield graphical contours.

First Stage

The cracking of the first stage fir tree necks 1 and 2 is obviously in a high stress concentration (Kt) region. For this reason, high fidelity models were needed for both 2D and 3D studies. Table 8 depicts the strain magnitudes predicted by the 2D model using nonlinear material properties, frictionless rollers, all lobes in contact, and no disk.

Table 9 on the other hand, shows the strains with the same 2D blade model in conjunction with frictionless gap elements and a disk model.

30

TABLE 8. FIRST STAGE 2D STRAIN WITHOUT DISK

Neck	Suction Side Strain (%)	Pressure Side Strain (%)
4	0.45	0.48
3	0.32	0.33
2	0.17	0.12
1	0.09	0.07

TABLE 9. FIRST STAGE 2D STRAIN WITH DISK

Neck	Suction Side Strain (%)	Pressure Side Strain (%)
4	0.49	0.45
3	0.47	0.50
2	0.49	0.56
1	0.40	0.44

Comparing these two tables, it is pretty convincing that any blade fir tree analysis without a disk is futile. The distribution of strains along each neck is completely different when disk effects are included. The highest strains for the first stage occurred in neck 2 pressure side with a magnitude of 0.56 percent. A closeup view of this neck showing the strain contours present can be seen in Figure 21. As shown previously in Figure 7, the MAR-M-246 DS material is highly susceptible to cracking in the presence of hydrogen if the temperature and strain level are right. In the room temperature regime, the material appears to tolerate almost no plastic strain prior to crack initiation. The yield strain of the parent material, as ground, is 0.57 percent. Thus, the predicted 2D strain of 0.56 percent would indicate that there is a reasonably high probability of cracks forming in this neck. When the effects of friction and fit-up tolerance are included, the neck strain is at least 0.80 percent and cracking would be assured.

The 3D first stage model was run using linear elastic properties, frictionless gap elements, all lobes in contact, and with a disk. Figure 22 depicts strain contours on five selected fir tree sections from the downstream face (also known as trailing edge TE) to the upstream face (also known as leading edge LE). Figure 23 shows only the center section extracted from the model. This section developed the largest strains in the fir tree and the location correlates with test hardware cracking. Table 10 reveals these strain levels for each neck.

The predicted maximum strain level, therefore, from the 3D analysis is 0.44 percent. This is well below the yield strain of the parent material (0.57 percent) where cracking is initiated. Again, if the effects of friction and fit-up tolerance are
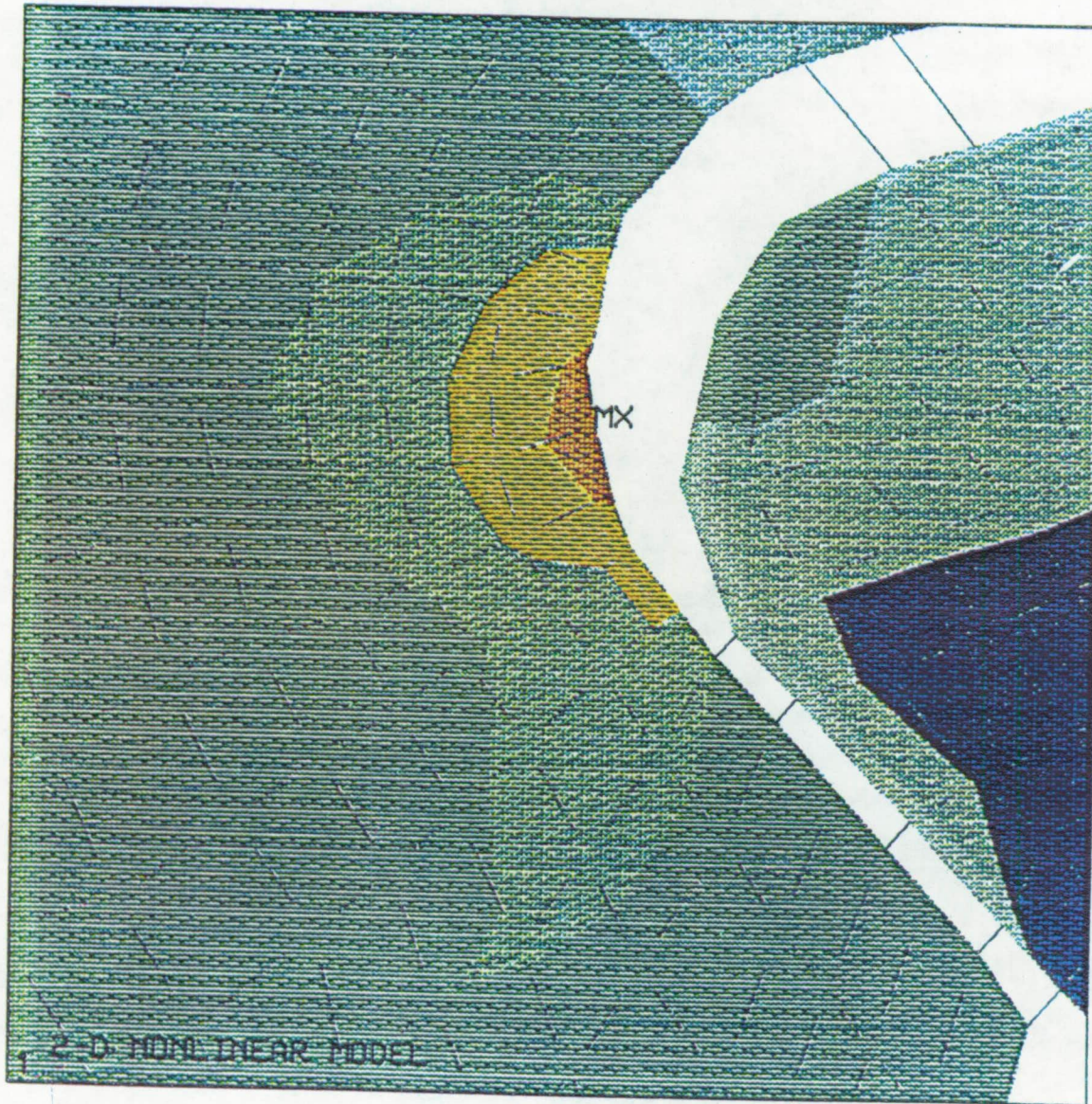
Figure 21. First-stage 2D strain contour.

ANSYS 4.2.2
SEP 24 1987
9:56:15
PLOT NO. 117
POST1 STRESS
STEP=2
ITER=15
PS1

ZV=1
DIST=.538
XF=.601
YF=.4
ZF=4.05
MX=.00446
MN=.000148
.000306
.000806
.00131
.00181
.00231
.00281
.00331
.00381
.00431
.00431

FIRST STAGE FIRTREE W/DISK FACE 1 8 8, 15, 23, 30

FTEE.   LTEE.

(FPL SS PRESSURE+SPEED+THERMAL)

Figure 22. First stage 3D strain contour.

```
        ANSYS  4.2
     SEP 24 1987
      9:52:14
     PLOT NO.    8
     POST1 STRESS
     STEP=2
     ITER=15
     PS1

     ZV=1
     DIST=.164
     XF=.617
     YF=.394
     ZF=4.05
     MX=.00446
     MN=.000332
     .000398
     .000898
     .0014
     .0019
     .0024
     .0029
     .0034
     .0039
     .0044
     .0049
```

FIRST STAGE FIRTREE W/DISK- FACE 15(CENTER)

*

*PRESSURE SIDE   SUCTION SIDE
     (FPL SS PRESSURE+SPEED+THERMAL)

Figure 23.   First-stage 3D section strain contour.

TABLE 10. FIRST-STAGE 3D STRAIN WITH DISK

Neck	Suction Side Strain (%)	Pressure Side Strain (%)
4	0.38	0.23
3	0.32	0.25
2	0.33	0.35
1	0.40	0.44

included, the neck strain would be at least 0.65 percent and cracking could occur. Figure 24 shows the same center section with the predicted temperature profile contoured. This chart indicates temperatures near -100°F in the high stress areas. Thus, the results of the 3D first-stage analysis indicate that crack initiation would probably be most likely to occur when a fit-up tolerance is introduced. This fact along with potentially low temperatures may well explain the minimal occurrence rate at which this particular crack has surfaced on actual test hardware.

One of the primary design modifications that has been implemented is shot peening of the fir tree region. Figure 25 shows plastic strain-to-crack initiation test results for the as-ground MAR-M-246 material versus MAR-M-246 shot peened. The shot peened material now has a yield strain of 0.52 percent as compared to 0.57 percent for as-ground. The big improvement lies in the fact that high compressive residual strains are present in the shot-peened condition as illustrated by Figure 26 for MAR-M-247. This data, obtained from X-ray defraction techniques, indicates significant residual compression 3 to 4 mils below the surface. Figure 27 relates from testing the shot-peened surface material stress-strain curve to the parent material stress-strain curve. The most important fact is that the parent material strain-to-crack initiation is 0.57 percent (yield), while the shot-peened material strain-to-crack initiation is 1.37 percent. The 1.37 percent strain includes 0.52 percent yield capability plus 0.85 percent residual compressive strain. Utilizing the 3D linear elastic analytical results, the following factors of safety against cracking exist for shot-peened blades:

FACTOR OF SAFETY = 1.37% / 0.44% = 3.11
(for frictionless,
uniform fit-up)

FACTOR OF SAFETY = 1.37% / 0.653% = 2.09
(for friction plus
non-uniform fit-up)

With a factor of safety against cracking analytically established, the actual LCF life now becomes of interest. Figure 28 depicts some LCF data for MAR-M-246 DS in high pressure hydrogen near room temperature [2]. Because of the limited number of data points and the fact that the LCF data forms such a flat curve, the predicted
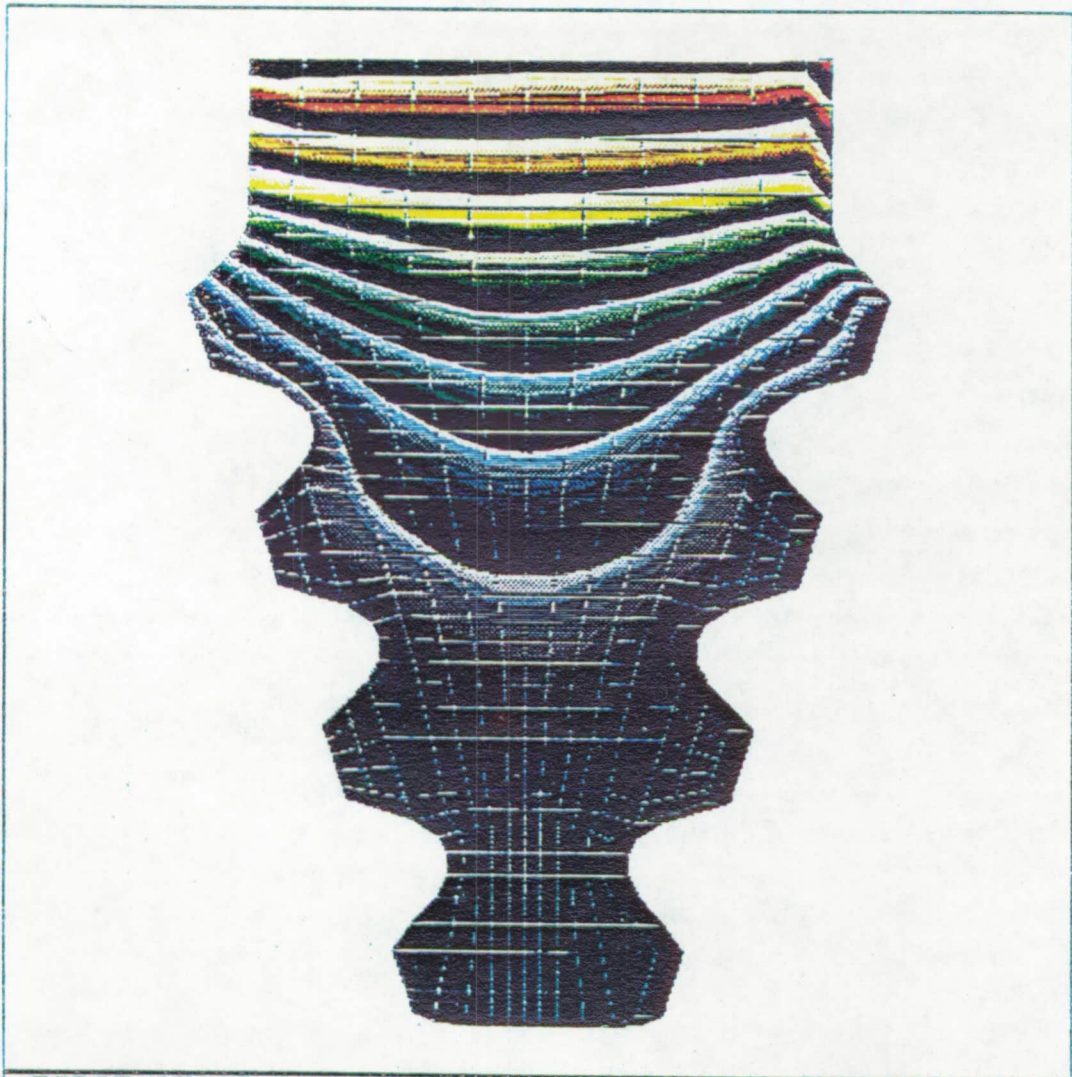
ANSYS 4.2
SEP 24 1987
9:52:23
PLOT NO. 9
POST1 STRESS
STEP=2
ITER=15
TEMP

XV=1
DIST=.227
XF=.617
YF=.394
ZF=4.05
MX=683
MN=-312
-215
-115
-14.5
85.5
185
285
385
485
585
635

ORIGINAL PAGE
COLOR PHOTOGRAPH

FIRST STAGE FIRTREE W/DISK- FACE 15(CENTER)

*PRESSURE SIDE   SUCTION SIDE
        (FPL SS PRESSURE+SPEED+THERMAL)

Figure 24. First-stage 3D section temperatures.

PLASTIC STRAIN-TO-CRACK INITIATION
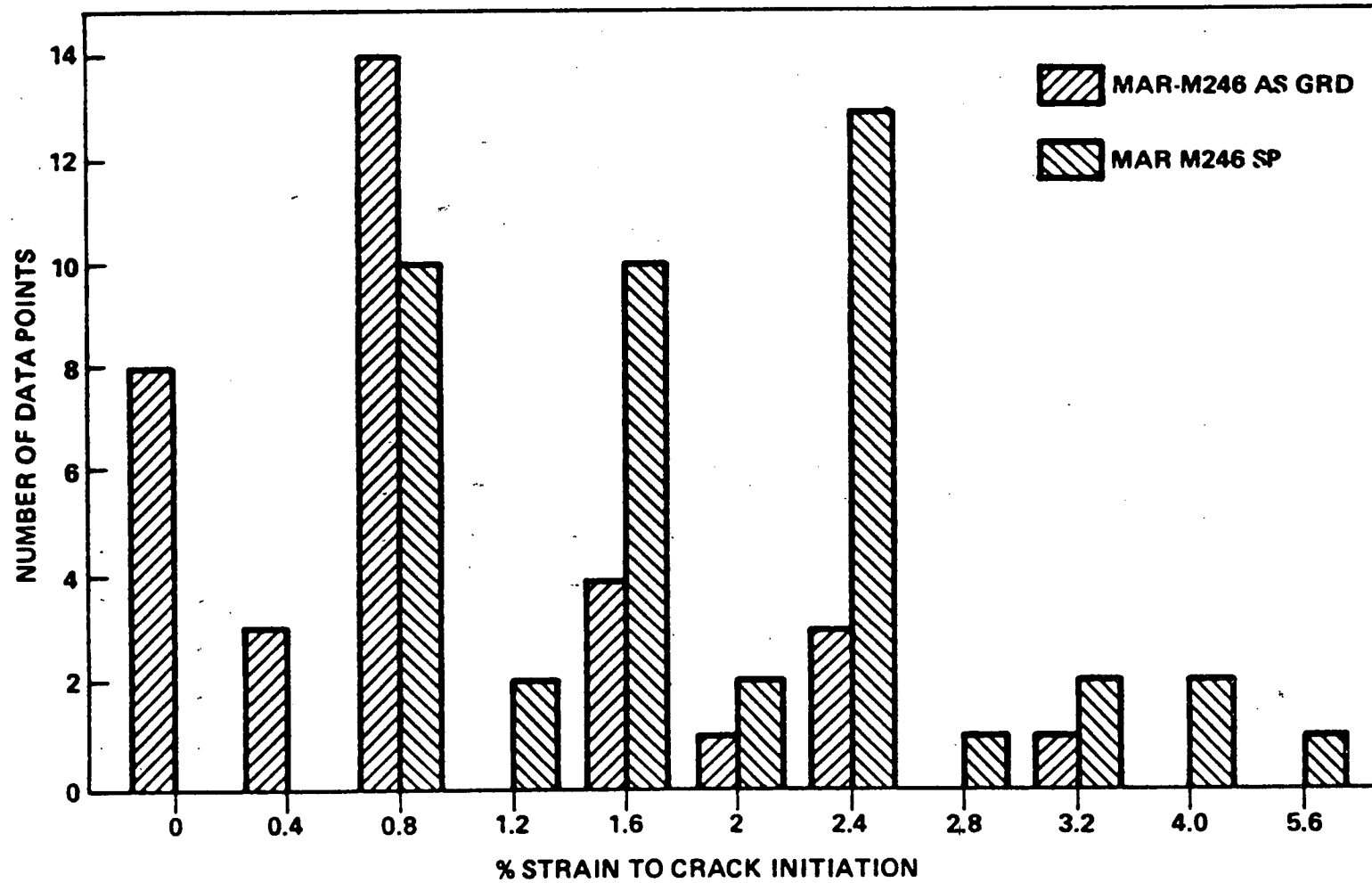## IN 5000 PSI HYDROGEN

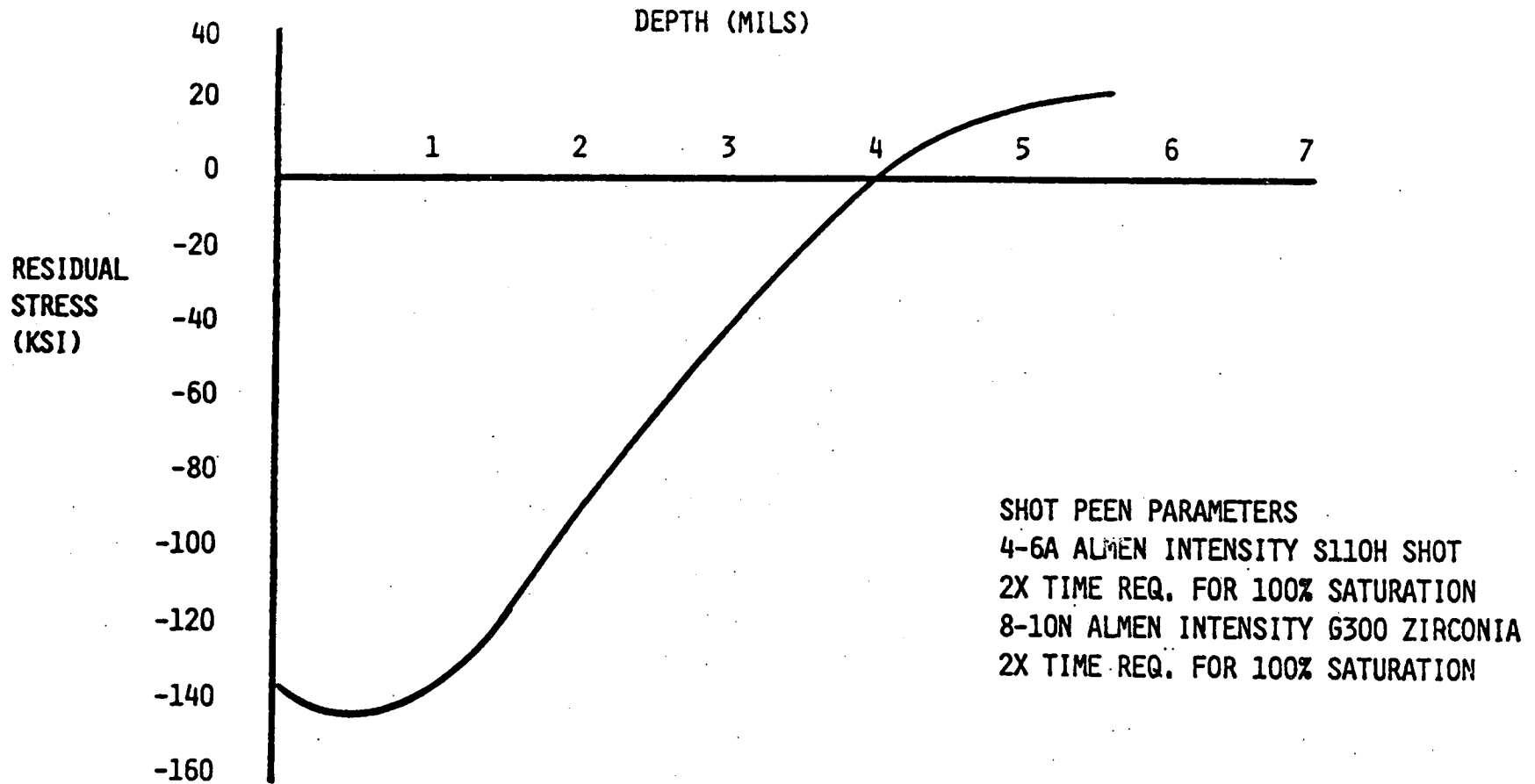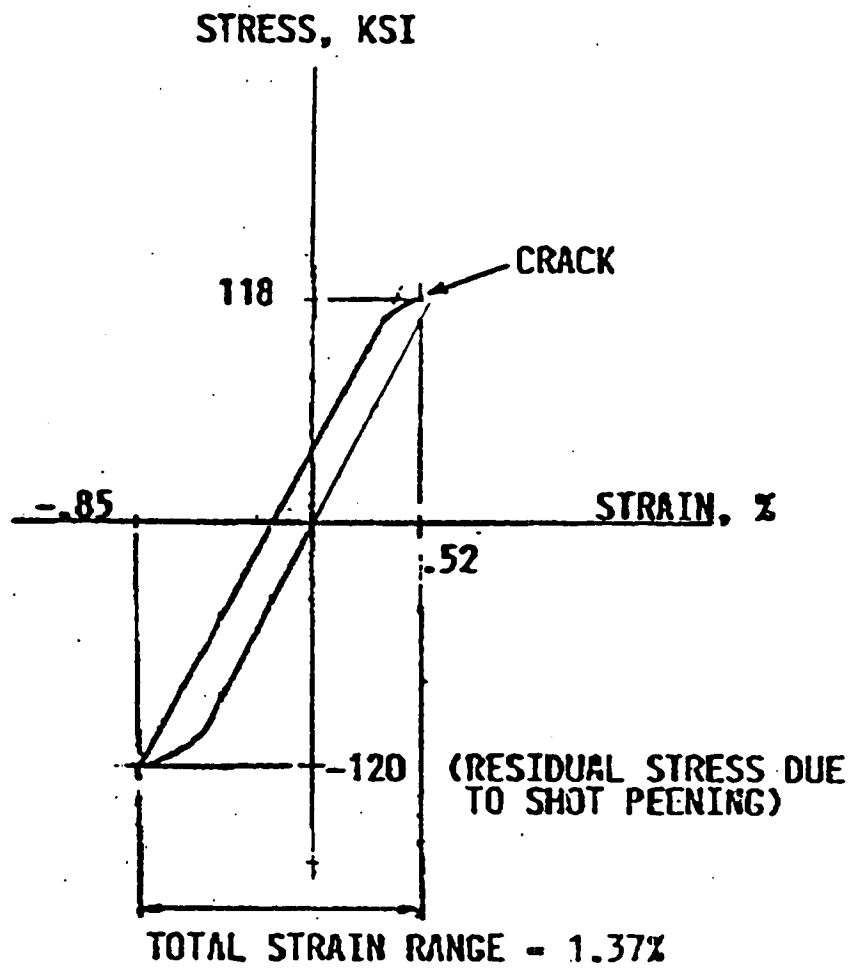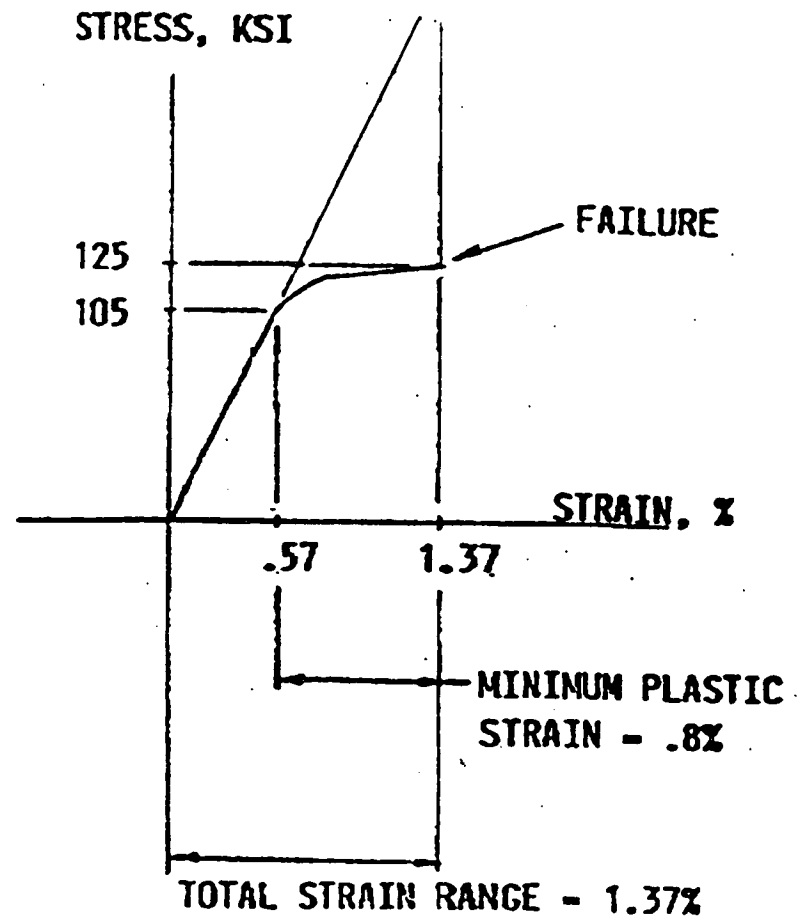Figure 25.   MAR-M-246 as-ground versus shot peened.

Figure 26. Shot-peened MAR-M-247 residual stress.

SURFACE MATERIAL

PARENT MATERIAL

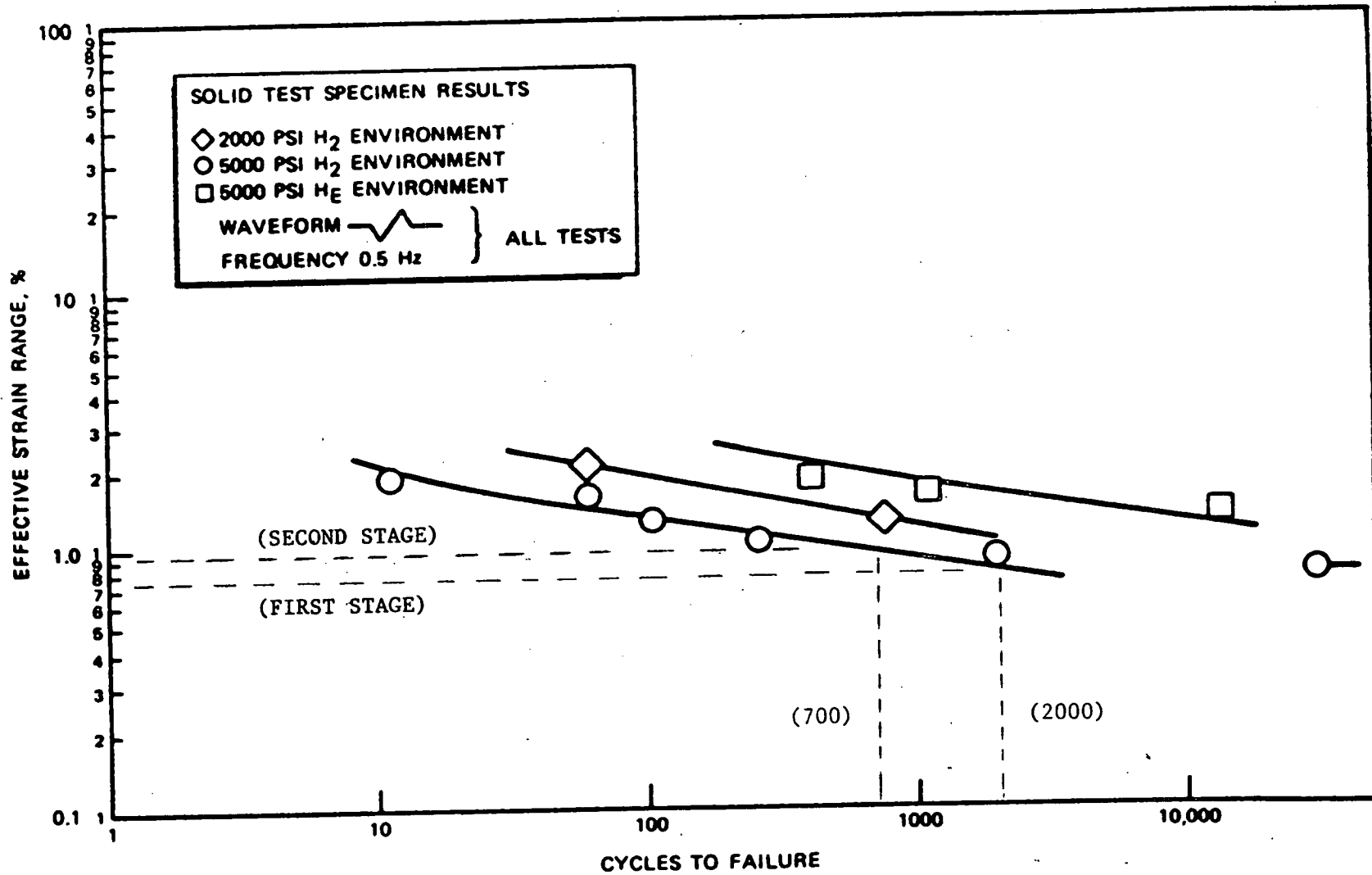Figure 27. MAR-M-246 test of shot-peened flat plate.

Figure 28. MAR-M-246 DS LCF data.

strain level for the first stage is multiplied by 1.15 prior to deriving life. This approach produces a 0.75 percent strain range and an associated LCF life of 2000 cycles. With a service life factor of four, the predicted life is 500 cycles.

Second Stage

The second-stage fir tree downstream face/corner cracking problem required reasonable model fidelity in the high stress concentration (Kt) areas as well as across the upper fir tree face for both 2D and 3D models. Table 11 tabulates the strain values predicted by the 2D model using nonlinear material properties, frictionless gap elements, all lobes in contact, and with a disk.
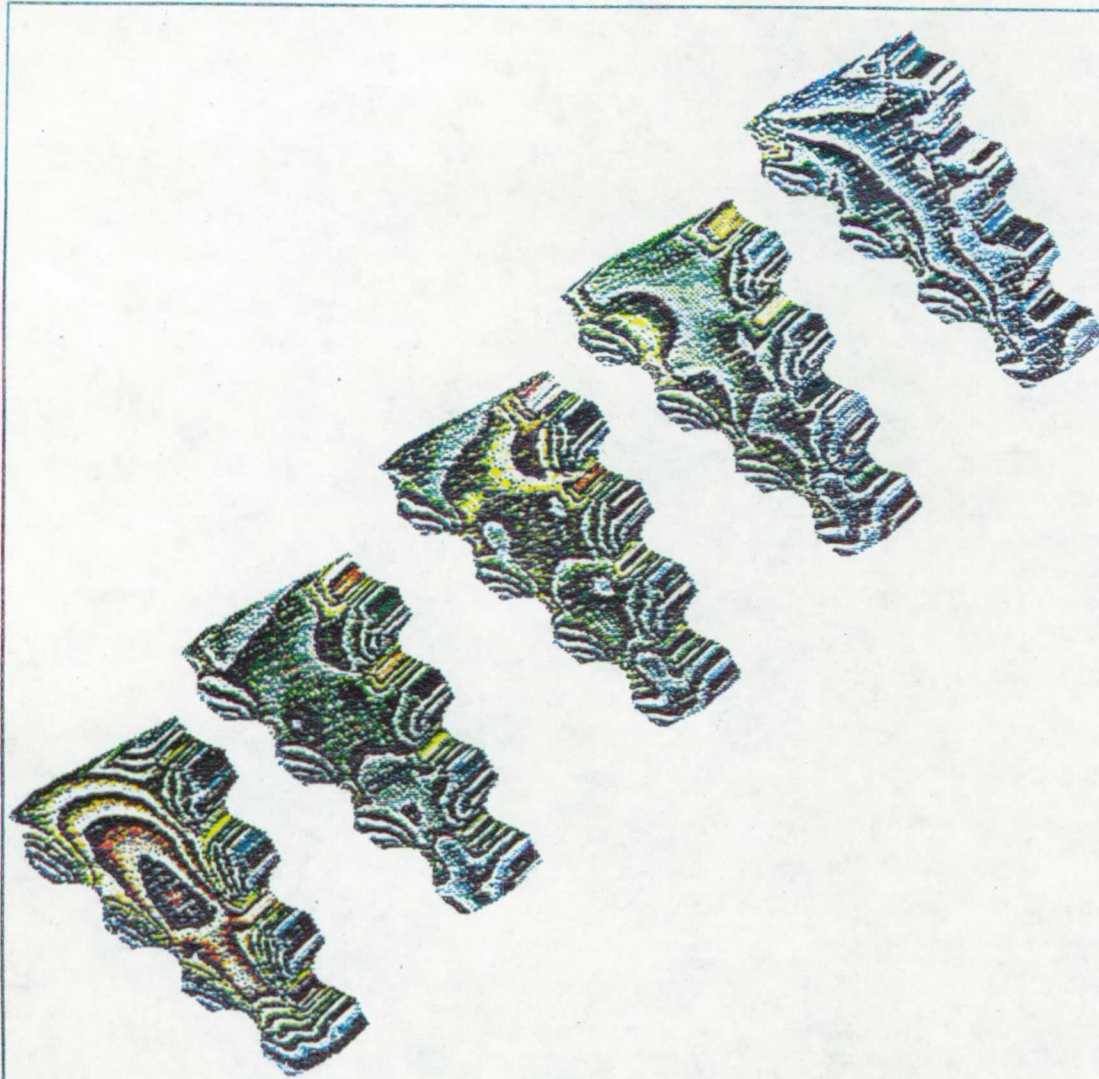
TABLE 11. SECOND-STAGE 2D STRAIN WITH DISK

Neck	Suction Side Strain (%)	Pressure Side Strain (%)
4	0.47	0.44
3	0.38	0.58
2	0.38	0.64
1	0.34	0.48

The 2D analysis friction and fit-up tolerance studies indicated increases in strains of 10 percent and 10 to 15 percent, respectively. With this in mind, these 2D results could produce at least 0.80 percent strain. This is quite sufficient to initiate cracking in room temperature environments. The 2D model, however, reveals that cracking could appear only in the neck 2 and 3 region on the pressure side. The reason for this is that the 2D model does not adequately account for the thermal gradient that exists normal to the downstream fir tree face. Only the 3D model can accurately predict this effect.

Like the first stage, the second stage 3D model was run using linear elastic material properties, frictionless gap elements, all lobes in contact, and a disk. Figure 29 shows the strain contour on five selected fir tree sections from the downstream face to the upstream face. Figure 30 depicts the downstream face section of elements that were extracted from the model. This section developed the highest strains in the fir tree and this location also is correlated by test hardware cracking evidence. Table 12 shows the strain levels predicted by the 3D model for the downstream face surface as well as 0.015 in. below the surface.

The main emphasis in Table 12 is to show the change in strain levels from 15 mils below the surface to the downstream surface itself. The prime loads driver here being a steep thermal gradient normal to the surface. Figure 31 shows the downstream face surface temperature contour which shows magnitudes near room temperature for the majority of the face. Figure 32 is a planer "slice" through the fir tree across neck 3. This "slice" clearly reveals the large thermal gradient (about 6000°F per inch) which leads to additional surface strain.

ANSYS 4.2
AUG 12 1987
11:08:12
PLOT NO.   23
POST1 STRESS
STEP=2
ITER=15
SP1

ZV=1
DIST=.55
XF=.601
YF=.4
ZF=3.98
MX=.0043
MN=.000211
.000257
.000757
.00126
.00176
.00226
.00276
.00326
.00376
.00426
.00476

ORIGINAL PAGE
COLOR PHOTOGRAPH

SECOND STAGE FIRTREE FACE 1,8,15,23,30

*T.E.   L.E.

(FPL SS PRESSURE+SPEED+THERMAL)

Figure 29.   Second-stage 3D strain contour.

```
                              ANSYS  4.2
                              AUG 14 1987
                              11:04:45
                              PLOT NO.    1
                              POST1 STRESS
                              STEP=2
                              ITER=15
                              SSEY

                              ZV=1
                              DIST=.164
                              XF=.117
                              YF=.566
                              ZF=3.98
                              MX=.00624
                              MN=-.00315
                              -.00246
                              -.00146
                              -.000456
                               .000544
                               .00154
                               .00254
                               .00354
                               .00454
                               .00554
                               .00654
```
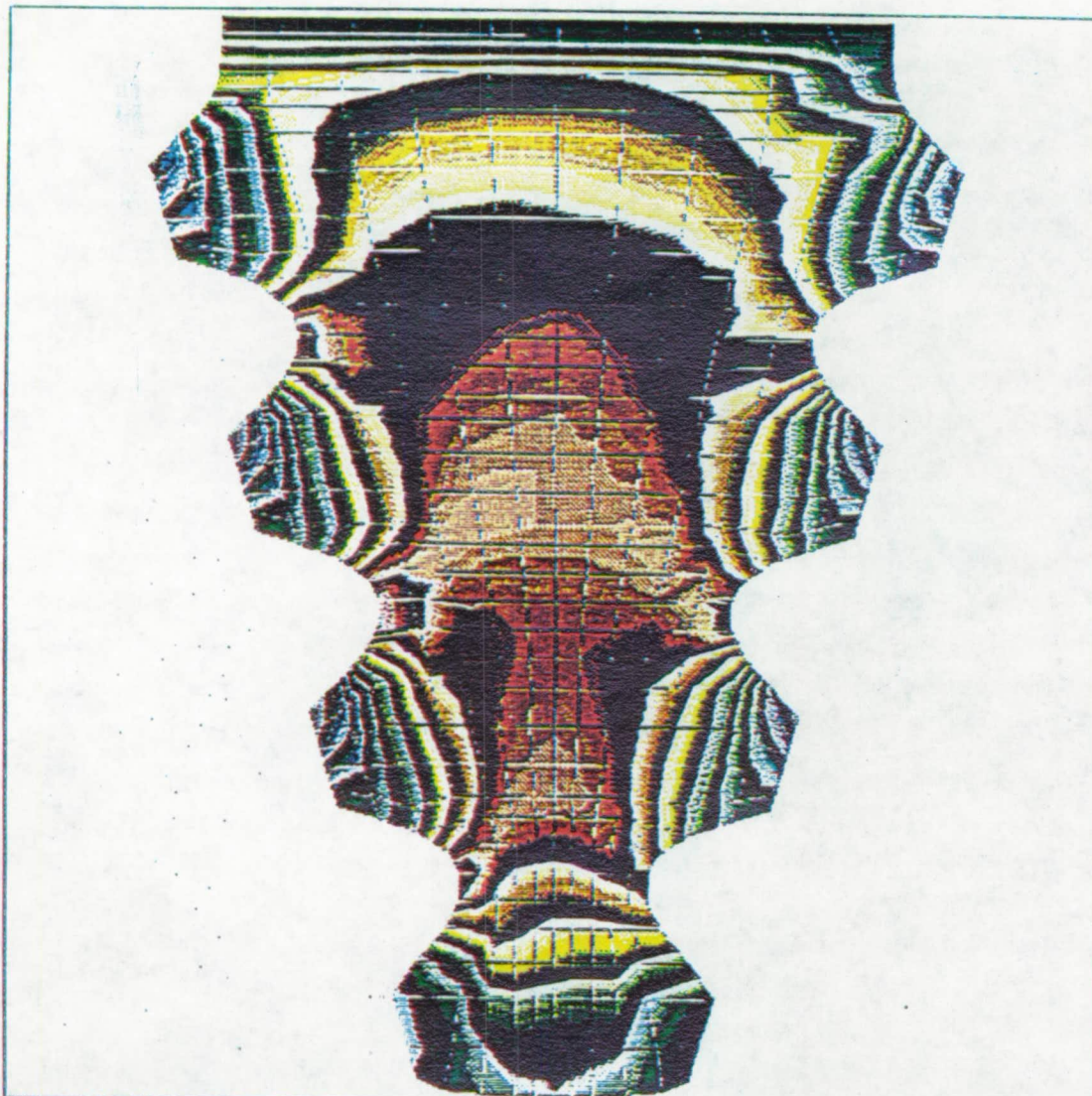
SECOND STAGE FIRTREE FACE 30 (T.E. SURFACE)
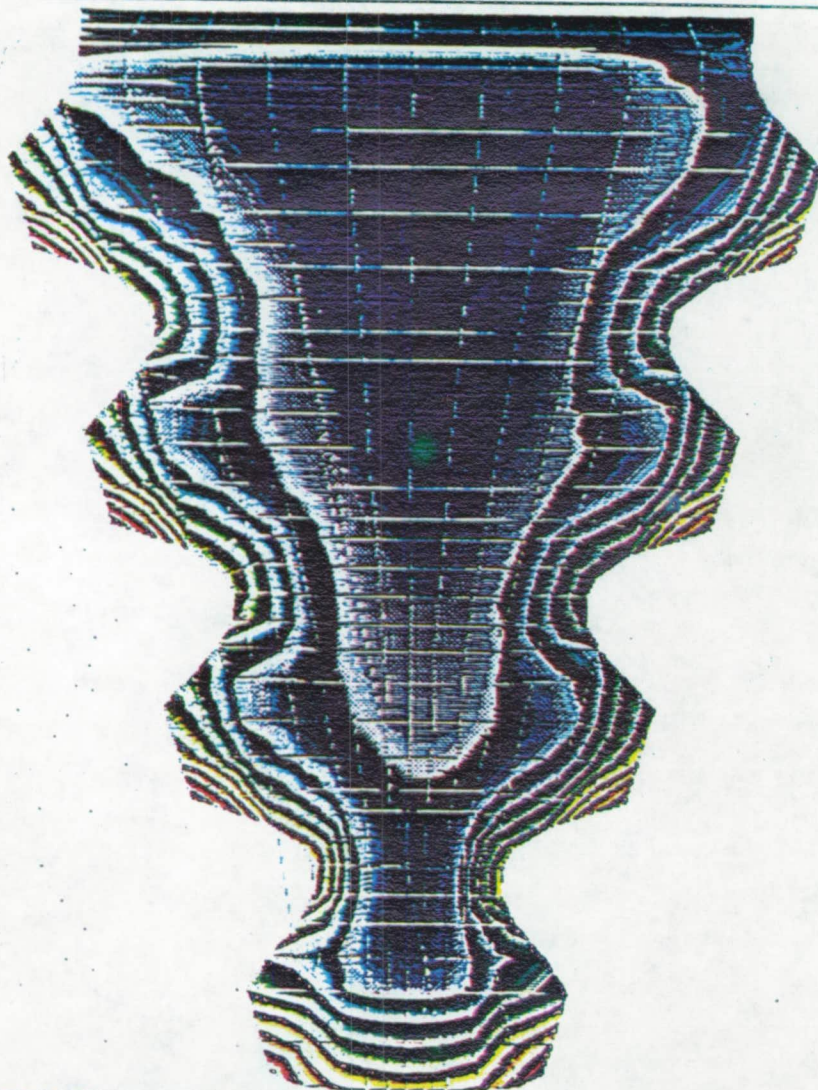
*PRESSURE SIDE   SUCTION SIDE
        (FPL SS PRESSURE+SPEED+THERMAL)

Figure 30.   Second-stage 3D section strain contour.

ANSYS 4.2
AUG 14 1987
11:04:52
PLOT NO.   2
POST1 STRESS
STEP=2
ITER=15
STEM

ZV=1
DIST=.164
XF=.117
YF=.566
ZF=3.98
MX=340
MN=-45.2
-8.82
30.2
69.2
108
147
186
225
264
303
342

ORIGINAL PAGE
COLOR PHOTOGRAPH

SECOND STAGE FIRTREE FACE 30 (T.E. SURFACE)

*PRESSURE SIDE   SUCTION SIDE
        (FPL SS PRESSURE+SPEED+THERMAL)

Figure 31.   Downstream face temperatures.
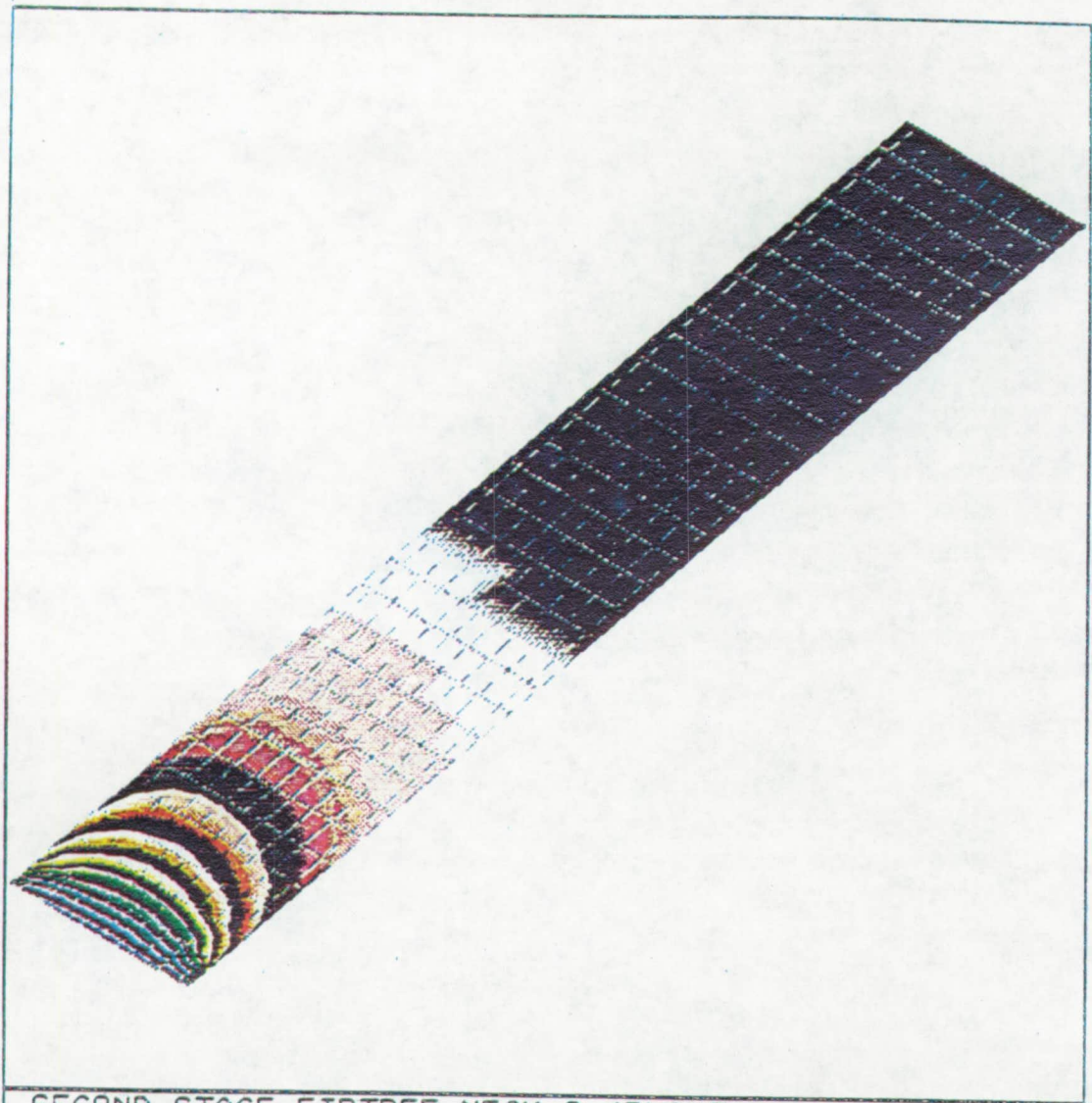
ANSYS 4.2
AUG 10 1987
9:54:43
PLOT NO. 26
POST1 STRESS
STEP=2
ITER=15
TEMP

ZV=1
DIST=.55
XF=.601
YF=.4
ZF=4.06
MX=980
MN=-44.5
55.9
159
262
365
468
571
674
777
880
983

SECOND STAGE FIRTREE NECK 3 (PLANE)

*T.E.   L.E.

(FPL SS PRESSURE+SPEED+THERMAL)

Figure 32. Downstream face thermal gradient.

TABLE 12. SECOND-STAGE 3D STRAIN WITH DISK

Neck	Suction Side Strain (%)		Pressure Side Strain (%)	
	0.015 in. Deep	Surface	0.015 in. Deep	Surface
4	0.27	0.25	0.21	0.27
3	0.23	0.45	0.34	0.56
2	0.33	0.55	0.40	0.64
1	0.30	0.47	0.37	0.60

The predicted maximum surface strain level from the second-stage model is 0.64 percent. This strain alone is sufficient to assure face/corner cracking. If the friction and fit-up tolerance effects are included, the strain would be at least 0.81 percent. Under the boundary conditions and load values utilized in this analysis, it would have to be concluded that every second-stage blade downstream face could develop hydrogen assisted LCF cracking. Indeed, there have been some tests where nearly every blade showed, as a minimum, some cracks after inspections with the scanning electron microscope (SEM).

As with the first stage, the second-stage fir tree is now shot peened in order to provide more plastic strain-to-crack capability as shown in Figure 25. Using the 3D linear elastic analytical results, the following factors of safety against cracking exist for the shot peened blades:

FACTOR OF SAFETY = 1.37% / 0.64% = 2.14
(for frictionless
uniform fit-up)

FACTOR OF SAFETY = 1.37% / 0.81% = 1.69
(for friction plus
non-uniform fit-up)

Using the same approach for LCF life as was used on the first stage, the maximum predicted strain range is 0.93 percent. The LCF data of Figure 28 results in a life of 700 cycles. With the service life factor of four, the predicted life is 175 cycles.

CONCLUSIONS

Utilization of large 2D and 3D finite element models of the SSME HPFTP first- and second-stage turbine blades for investigating the causes of potentially critical fir tree cracking has been accomplished. The analyses were accomplished using speed, pressure, and thermal loads that occur during the full power level (FPL-109%) of the engine. Analytical results indicate that the first-stage lobe neck hydrogen assisted

LCF cracking is unlikely to occur unless the effects of fit-up tolerances between the blade and rotor are present. The second-stage downstream face analysis predicts that hydrogen assisted LCF cracking is assured under the present thermal environment. However, with design modifications presently in place, these first- and second-stage analyses indicate that positive margins against fir tree cracking now exist. Some of these fir tree modifications include stress relieving and shot peening, providing more generous radii on corners, fit-up changes to improve load sharing, and reduction of acceptable material microporosity.

Recently, SSME turbine hardware from engine ground tests has yielded confirmation that the implemented design changes minimize the hydrogen assisted LCF crack occurrences on both stages. Based on the analytical effort described herein and the testing accomplished to date, building confidence in the life of the HPFTP blades is becoming a successful story in the process of NASA returning the shuttle to flight status.

REFERENCES

1. Rockwell International, Rocketdyne Division presentation BC 87-195, SSME Turbine Blade Review, August 18, 1987.

2. Rockwell International, Rocketdyne Division presentation BC-87-276, Material Properties Comparison-Single Crystal Alloy 1480-Directionally Solidified MAR-M-246, December 1987.

3. Lockheed Missiles and Space Company Technical Report, Assessment of HPFTP Turbine Blade Environment and Fatigue Life Study on the SSME, contract NAS8-32703, May 1981.

4. Marshall Space Flight Center letter EP26(86-79): Environments in the High Pressure Fuel Turbine, Huntsville, Alabama, October 20, 1986.

5. Marshall Space Flight Center letter EL51(133-87): Finite Element Thermal Analysis of the High Pressure Fuel Turbopump (HPFTP) Turbine Blade, Huntsville, Alabama, November 1987.

6. Marshall Space Flight Center letter EH23(86-147): MAR-M-246 and Waspaloy Material Properties for SSME Turbopump High Pressure Fuel Turbopump Turbine Blade Analysis, Huntsville, Alabama, December 1986.

7. Marshall Space Flight Center letter EH23(87-28): MAR-M-246 and Waspalloy Material Properties for SSME Turbopump High Pressure Fuel Turbopump Turbine Blade Analysis, Huntsville, Alabama, March 1987.

APPENDIX

Because of the core limitations on the Cray X-MP/44 core memory and the ANSYS wavefront solution size limitation, the substructured rotor could not be included in the existing blade model analysis. To circumvent this problem, the resulting substructured stiffnesses were utilized by the technique below to allow for more realistic rotor effective stiffness values. These stiffnesses, once calculated, were assigned to the respective gap elements which transfer loads across blade and rotor fir trees.

Writing the matrix form of the rotor structure:

$$
\begin{Bmatrix} F1 \\ F2 \\ \downarrow \\ Fn \end{Bmatrix}
=
\begin{bmatrix} K11 & K12 \longrightarrow Kln \\ K21 & K22 \\ \downarrow & \searrow \\ Knl & Knn \end{bmatrix}
\begin{Bmatrix} X1 \\ X2 \\ \downarrow \\ Xn \end{Bmatrix}
$$

where

Fi = force at node i

Xi = displacement at node i

Kij = stiffness at node i due load at node j

for node 1 on the rotor this can be written as

$$F1 = (K11)(X1) + (K12)(X2) + \ldots (Kln)(Xn)$$

and

$$K11 = \frac{F1}{X1} = (K11) + (K12)\frac{X12}{X1} + \ldots (Kln)\frac{Xn}{X1}$$

or

$$K11 = K11 + \sum_{j=1}^{n} (K1j)\frac{Xj}{X1}$$

where
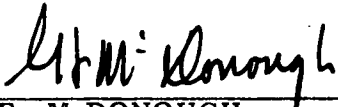
$K11$ = effective rotor gap element stiffness at node 1 .

At this point, relationships between nodal displacements (Xj and $X1$) were derived from previously run models. This technique was verified using the 2D blade/rotor model. The results of the all model compared identically to those of the substructured effective stiffness model.

APPROVAL

SPACE SHUTTLE MAIN ENGINE HIGH PRESSURE FUEL TURBOPUMP TURBINE BLADE CRACKING

By Henry Lee

The information in this report has been reviewed for technical content. Review of any information concerning Department of Defense or nuclear energy activities or programs has been made by the MSFC Security Classification Officer. This report, in its entirety, has been determined to be unclassified.

G. F. McDONOUGH
Director, Structures and Dynamics Laboratory